Journal of Alzheimer's Disease xx (20xx) x–xx
DOI 10.3233/JAD-181123
IOS Press

Combined Transcriptomics and Proteomics in Frontal Cortex Area 8 in Frontotemporal Lobar Degeneration Linked to *C9ORF72* Expansion

Pol Andrés-Benito[a,b], Ellen Gelpi[c,d], Mónica Povedano[g], Karina Ausín[h,i], Joaquín Fernández-Irigoyen[h,i], Enrique Santamaría[h,i] and Isidro Ferrer[a,b,e,f,*]

[a]*Neuropathology, Pathologic Anatomy Service, Bellvitge University Hospital - Bellvitge Biomedical Research Institute (IDIBELL), Hospitalet de Llobregat, Spain*

[b]*Biomedical Network Research Center on Neurodegenerative Diseases (CIBERNED), Institute of Health Carlos III, Hospitalet de Llobregat, Spain*

[c]*Neurological Tissue Bank of the Biobanc-Hospital Clínic-Institut d'Investigacions Biomèdiques August Pi i Sunyer (IDIBAPS), Barcelona, Spain*

[d]*Institute of Neurology, Medical University of Vienna, Vienna, Austria*

[e]*Department of Pathology and Experimental Therapeutics, University of Barcelona, Hospitalet de Llobregat, Spain*

[f]*Institute of Neurosciences, University of Barcelona, Barcelona, Spain*

[g]*Functional Unit of Amyotrophic Lateral Sclerosis (UFELA), Service of Neurology, Bellvitge University Hospital, Hospitalet de Llobregat, Spain*

[h]*IDISNA, Navarra Institute for Health Research, Pamplona, Spain*

[i]*Clinical Neuroproteomics group and Proteored-ISCIII, Proteomics Unit, Navarrabiomed, Department of Health, Public University of Navarra, Pamplona, Spain*

Accepted 31 January 2019

Abstract.

Background: Frontotemporal lobar degeneration with TDP-43 immunoreactive inclusions (FTLD-TDP) may appear as sporadic (sFTLD-TDP) or linked to mutations in various genes including expansions of the non-coding region of *C9ORF72* (c9FTLD).

Objective: Analysis of differential mRNA and protein expression in the frontal cortex in c9FLTD and evaluation with previous observations in frontal cortex in sFTLD-TDP and amyotrophic lateral sclerosis with TDP-43 inclusions.

Methods: Microarray hybridization and mass spectrometry-based quantitative proteomics followed by RT-qPCR, gel electrophoresis, and western blotting in frontal cortex area 8 in 19 c9FTLD cases and 14 age- and gender-matched controls.

Results: Microarray hybridization distinguish altered gene transcription related to DNA recombination, RNA splicing regulation, RNA polymerase transcription, myelin synthesis, calcium regulation, and ubiquitin-proteasome system in c9FTLD; proteomics performed in the same tissue samples pinpoints abnormal protein expression involving apoptosis, inflammation,

*Correspondence to: Prof. Isidro Ferrer, Department of Pathology and Experimental Therapeutics, University of Barcelona, Campus Bellvitge, c/Feixa Llarga sn, 08907 L'Hospitalet de Llobregat, Spain. Tel.: +34 93 4035808; E-mail: 8082ifa@gmail.com.

ISSN 1387-2877/19/$35.00

metabolism of amino acids, metabolism of carbohydrates, metabolism of membrane lipid derivatives, microtubule dynamics, morphology of mitochondria, neuritogenesis, neurotransmission, phagocytosis, receptor-mediated endocytosis, synthesis of reactive oxygen species, and calcium signaling in c9FTLD.

Conclusion: Transcriptomics and proteomics, as well as bioinformatics processing of derived data, reveal similarly altered pathways in the frontal cortex in c9FTLD, but different RNAs and proteins are identified by these methods. Combined non-targeted '-omics' is a valuable approach to deciphering altered molecular pathways in FTLD provided that observations are approached with caution when assessing human postmortem brain samples.

Keywords: C9ORF72, frontotemporal lobar degeneration, FTLD-TDP, gene expression, proteomics

INTRODUCTION

Frontotemporal lobar degeneration with TDP-43 inclusions (FTLD-TDP) is manifested by behavioral-dysexecutive disorder, primary progressive aphasia, and/or motor disorders including motor neuron disease due to frontal and temporal atrophy, as well as variable involvement of the basal ganglia, substantia nigra, and spinal cord. Neuron loss in the cerebral cortex, microvacuolation in the upper cortical layers, astrogliosis, and TDP-43-immunoreactive inclusions in the nucleus and/or cytoplasm of neurons and oligodendocytes and in neuropil threads, are the main microscopical alterations [1–4]. Some cases are sporadic (sFTLD-TDP) whereas others are genetic, often familial (fFTLD-TDP) and linked to mutations in various genes including *GRN* (progranulin), *C9ORF72* (chromosome 9 open reading frame 72), *TARDP* (TAR DNA-binding protein), *VCP* (valosin-containing protein), *CHMBP2* (charged multivesicular body protein 2), and *UBQLN* (ubiquilin 2), among others [4, 5–8]. The presence of TDP-43 inclusions in amyotrophic lateral sclerosis (ALS), together with the fact that mutations in the same genes, excepting *GRN*, may be causative of ALS, suggests that ALS and FTLD-TDP are within the same disease spectrum [9–13].

C9ORF72 expansions produce haploinsufficiency of C9*orf*72 protein, RNA foci sequestering of various RNA-binding proteins, dipeptide repeat protein inclusions probably sequestering additional proteins, abnormal protein binding, TDP-43 aggregation and loss of function, nucleocytoplasmic transport defects, RNA mis-splicing, DNA damage, abnormal stress granule dynamics, and altered autophagy, among others [8, 14–41].

Complementary information has been gained from the application of transcriptomics and proteomics in FTLD-TDP and ALS [42–45] but studies including FTLD linked to *C9ORF72* expansion (c9FTLD) are scarce [46]. The present study was designed to gain understanding about c9FTLD pathogenesis by using microarray hybridization and mass spectrometry-based quantitative proteomics in frontal cortex area 8 postmortem samples. Data were then processed using bioinformatics methods to identify altered molecular pathways and their interactions. Finally, data obtained in c9FTLD were compared with those previously obtained in the same cortical region in sFTLD-TDP and sALS.

MATERIAL AND METHODS

Human cases

Postmortem fresh-frozen frontal cortex (FC) (Brodmann area 8) samples were obtained from the Institute of Neuropathology HUB-ICO-IDIBELL Biobank and the Hospital Clinic-IDIBAPS Biobank following the guidelines of Spanish legislation on this matter and approval of the local ethics committees. The postmortem interval between death and tissue processing was between 2 and 18 h. One hemisphere was immediately cut in coronal sections, 1 cm thick, and selected areas of the encephalon were rapidly dissected, frozen on metal plates over dry ice, placed in individual air-tight plastic bags, and stored at –80°C until use for biochemical studies. The other hemisphere was fixed by immersion in 4% buffered formalin for 3 weeks for morphological studies. FTLD-TDP cases were diagnosed following well-established criteria [1]. All cases bore *C9ORF72* repeat expansion (more than 30 intronic hexanucleotide repeats). TDP-43-immunoreactive inclusions were found in the frontal cortex in every case; these were neuronal cytoplasmic inclusions mainly in layer II but also in the deeper layers in some cases, together with dystrophic neurites corresponding to types A and B [47], and sequential pattern II-III [48]. Patients with associated pathologies, including middle or late stages of Alzheimer's and Parkinson's diseases, and those with

vascular diseases, neoplastic disorders affecting the nervous system, metabolic syndrome, hypoxia, and prolonged axonal states such as those occurring in intensive care units, were excluded. The whole series included 19 familial cases of fFTLD associated with *C9ORF72* mutation, henceforth named c9FTLD for practical purposes (mean age 70 years; 10 men and 9 women), and 14 cases (mean age 67 years; 8 men and 6 women) not suffering from neurologic or psychiatric diseases, and without abnormalities in the neuropathologic examination, which were assessed in parallel as age-matched controls (Table 1). Details of the clinical symptoms were very brief in the accompanying data provided with the brain samples used for study. Apathy, loss of empathy, disinhibition, executive dysfunction, memory loss, hallucinations, and delusions were common, often accompanied by motor neuron disease; parkinsonism and progressive aphasia were reported in some cases.

Table 1
Summary of the thirty-three cases analyzed, including frontal cortex area 8 of 14 controls and 19 fFTLD cases. c9FTLD, familial FTLD linked to C9orf72 expansion; F, female; M, male; PMD, postmortem delay (hours, minutes); RIN, RNA integrity number

Case	Sex	Age	Diagnosis	PMD	RIN
1	M	66	Control	18 h 00 min	6.4
2	M	61	Control	03 h 40 min	7.0
3	M	62	Control	05 h 45 min	5.0
4	M	74	Control	06 h 40 min	7.2
5	M	65	Control	05 h 15 min	6.8
6	F	64	Control	02 h 15 min	5.0
7	M	63	Control	08 h 05 min	7.1
8	F	79	Control	03 h 35 min	6.8
9	F	67	Control	05 h 20 min	6.2
10	M	70	Control	03 h 45 min	7.2
11	M	52	Control	04 h 40 min	7.2
12	F	52	Control	05 h 45 min	5.1
13	F	82	Control	07 h 35 min	5.2
14	F	74	Control	02 h 45 min	5.7
15	M	69	c9FTLD	11 h 30 min	6.5
16	F	69	c9FTLD	13 h 15 min	5.4
17	M	68	c9FTLD	02 h 30 min	6.8
18	M	61	c9FTLD	07 h 45 min	6.9
19	M	66	c9FTLD	15 h 15 min	7.9
20	F	55	c9FTLD	03 h 15 min	8.7
21	M	69	c9FTLD	05 h 00 min	6.1
22	F	75	c9FTLD	17 h 30 min	7.5
23	F	92	c9FTLD	09 h 15 min	7.1
24	F	58	c9FTLD	11 h 00 min	8.4
25	F	66	c9FTLD	11 h 30 min	8,1
26	M	73	c9FTLD	15 h 30 min	6.2
27	F	69	c9FTLD	12 h 30 min	5.9
28	F	57	c9FTLD	03 h 40 min	7.2
29	M	80	c9FTLD	12 h 00 min	8.0
30	F	57	c9FTLD	08 h 00 min	6.9
31	M	88	c9FTLD	05 h 00 min	7.3
32	M	69	c9FTLD	05 h 45 min	7.1
33	M	80	c9FTLD	08 h 30 min	6.5

RNA purification

RNA from frozen frontal cortex area 8 was extracted following the instructions of the supplier (RNeasy Mini Kit, Qiagen® GmbH, Hilden, Germany). RNA integrity and 28S/18S ratios were determined with the Agilent Bioanalyzer (Agilent Technologies Inc, Santa Clara, CA, USA) to assess RNA quality combined with DNase digestion to avoid extraction and later amplification of genomic DNA, and the RNA concentration was evaluated using a NanoDrop™ Spectrophotometer (Thermo Fisher Scientific, Waltham, MA, USA). RIN values are shown in Table 1. Special care was taken to assess premortem and postmortem factors which may interfere with RNA processing [49].

Microarray hybridization

Samples were analyzed by microarray hybridization with Human Clariom™ D Assay kit and GeneChip WT Plus Reagent Kit, and microarray 7000G platform from Affymetrix® (Affymetrix, Santa Clara, CA, USA) with a capacity to detect more than 540,000 transcripts. Preprocessing of raw data and statistical analyses were performed using bioconductor packages in an R programming environment for genes [50] which enabled data preprocessing for differential gene expression analysis and enrichment analysis. Gene selection was based upon their values using a test for differential expression between two classes (Student's *t*-test). Genes differentially expressed showed an absolute fold change >2.0 in combination with a p-value ≤ 0.05.

RT and q-PCR

Complementary DNA (cDNA) preparation used the High-Capacity cDNA Reverse Transcription kit (Applied Biosystems, Foster City, CA, USA) following the protocol provided by the supplier. Parallel reactions for each RNA sample were run in the absence of MultiScribe Reverse Transcriptase to assess the lack of contamination of genomic DNA. TaqMan RT-qPCR assays were performed in duplicate for each gene on cDNA samples in 384-well optical plates using an ABI Prism 7900 Sequence Detection System (Applied Biosystems). For each 10 μL TaqMan reaction, 4.5 μL cDNA was mixed with 0.5 μL 20× TaqMan Gene Expression Assays and 5 μL of 2× TaqMan Universal PCR

Table 2
Genes, gene symbols, and TaqMan probes used for the study of gene expression including probe for normalization (*GUS*-β)

Gene	Full name	Reference
C9ORF72	*Chromosome 9 Open Reading Frame 72*	Hs00376619_m1
CNP	*2′,3′-Cyclic Nucleotide 3′ Phosphodiesterase*	Hs00263981_m1
DDX3Y	*DEAD-Box Helicase 3 Y-Linked*	Hs00190539_m1
EIF1AY	*Eukaryotic Translation Initiation Factor 1A Y-Linked*	Hs01040047_m1
GPN2	*GPN-Loop GTPase 2*	Hs00216252_m1
GUS-β	*β-glucuronidase*	Hs00939627_m1
MAG	*Myelin Associated Glycoprotein*	Hs01114387_m1
MAL	*Mal, T-Cell Differentiation Protein*	Hs00360838_m1
MBP	*Myelin Basic Protein*	Hs00921945_m1
MOBP	*Myelin-Associated Oligodendrocyte Basic Protein*	Hs01094434_m1
MOG	*Myelin Oligodendrocyte Glycoprotein*	Hs01555268_m1
MYRF	*Myelin Regulatory Factor*	Hs00973739_m1
NG2	*Neural/glial antigen 2*	Hs00426981_m1
OLIG1	*Oligodendrocyte Transcription Factor 1*	Hs00744293_s1
OLIG2	*Oligodendrocyte Lineage Transcription Factor 2*	Hs00377820_m1
PLP1	*Proteolipid Protein 1*	Hs00166914_m1
SCARNA2	*Small Cajal Body-Specific RNA 2*	Hs04232660_s1
SOX-10	*SRY-Box 10*	Hs00366918_m1
TARDBP	*TAR DNA Binding Protein*	Hs00606522_m1
UBR5	*Ubiquitin Protein Ligase E3 Component N-Recognin 5*	Hs00210750_m1

Master Mix (Applied Biosystems) [51]. Table 2 shows identification numbers and names of selected TaqMan probes. Values for glucuronidase-β (*GUS*-β) were used as internal controls for normalization. The selection of this housekeeping gene was based on previous data showing its low vulnerability in the brain in several human neurodegenerative diseases [52]. The parameters of the reactions were 50°C for 2 min, 95°C for 10 min, and 40 cycles of 95°C for 15 s, and 60°C for 1 min. Finally, all TaqMan PCR data were captured with Sequence Detection Software (SDS version 2.2.2, Applied Biosystems). The double-delta cycle threshold (ΔΔCT) method was used to analyze the data. Results were analyzed using Student's *t*-test [50].

Proteomic analysis

Sample preparation for proteomic analysis

Frozen samples of frontal cortex from eight c9FTLD and eight controls of the same case series were homogenized in lysis buffer containing 7 M urea, 2 M thiourea, and 50 mM DTT. The homogenates were spun down at 100,000 ×g for 1 h at 15°C. Protein concentration was measured in the supernatants with the Bradford assay kit (Biorad, Hercules, CA, USA).

Label free LC-MS/MS

The protein extract for each sample was diluted in Laemmli sample buffer and loaded into a 0.75 mm thick polyacrylamide gel with a 4% stacking gel cast over a 12.5% resolving gel. The run was stopped as soon as the front entered 3 mm into the resolving gel so that the whole proteome became concentrated in the stacking/resolving gel interface. Bands were stained with Coomassie Brilliant Blue and excised from the gel. Protein enzymatic cleavage (20 μg) was carried out with trypsin (1:20, w/w, Promega, Madison, WI, USA) at 37°C for 16 h. Purification and concentration of peptides was performed using C18 Zip Tip Solid Phase Extraction (Millipore, Burlington, MA, USA). Peptide mixtures were separated by reverse phase chromatography using an Eksigent nanoLC ultra 2D pump fitted with a 75 μm ID column (Eksigent 0.075 × 250). Samples were first loaded for desalting and concentration into a 0.5 cm length 100 μm ID pre-column packed with the same chemistry as the separating column. Mobile phases were 100% water, 0.1% formic acid (FA) (buffer A), and 100% acetonitrile 0.1% FA (buffer B). Column gradient was developed in a two-step gradient from 5% B to 25% B for 210 min and 25%B to 40% B for 30 min. The column was equilibrated in 95% B for 9 min and 5% B for 14 min. During the entire process, pre-column was in line with column, and the flow maintained all along the gradient at 300 nl/min. Eluting peptides from the column were analyzed using an AB Sciex 5600 Triple-TOF system (Sciex). Information data were acquired upon a survey scan performed in a mass range from 350 m/z up to 1,250 m/z in a scan time of 250 ms. The top 35 peaks were selected for fragmentation. Minimum accumulation time for MS/MS was set at 100 ms, yielding a total cycle time

of 3.8 s. Product ions were scanned in a mass range from 230 m/z up to 1,500 m/z and excluded for further fragmentation for 15 s.

Peptide identification and quantification

MS/MS data acquisition was performed using Analyst 1.7.1 (Sciex) and spectra files were processed through Protein Pilot Software (v.5.0-Sciex) using Paragon™ algorithm (v.4.0.0.0) for database search and Progroup™ for data grouping, and then searched against the concatenated target-decoy UniProt proteome reference Human database (Proteome ID: UP000005640, 70902 proteins, December 2015). False discovery rate was identified using a nonlineal fitting method [53], and displayed results were those reporting a 1% global false discovery rate or better. The peptide quantification was performed using the Progenesis LC–MS software (version 2.0.5556.29015, Nonlinear Dynamics, Newcastle, UK). Using the accurate mass measurements from full survey scans in the TOF detector and the observed retention times, runs were aligned to compensate for between-run variations in our nanoLC separation system. To this end, all runs were aligned to a reference run automatically chosen by the software, and a master list of features considering m/z values and retention times was generated. The quality of these alignments was manually supervised with the help of quality scores provided by the software. The peptide identifications were exported from Protein Pilot software and imported into Progenesis LC-MS software, where they were matched to the respective features. Output data files were managed using Perseus Software for subsequent statistical analyses and representation [54]. Proteins identified by site (identification based only on a modification), reverse proteins (identified by decoy database), and potential contaminants were filtered out. Proteins quantified with at least two unique peptides, a *p*-value lower than 0.05 and an absolute fold change of <0.77 (downregulation) or >1.3 (upregulation) in linear scale, were considered to be significantly differentially expressed. MS raw data and search results files were deposited in the ProteomeXchange Consortium (http://proteomecentral.proteomexchange.org) via the PRIDE partner repository with the dataset identifiers PXD011713.

Proteome bioinformatic analysis

The specifically dysregulated regulatory/metabolic networks identified in c9FTLD were analyzed with the use of QIAGEN's Ingenuity® Pathway Analysis (IPA) (QIAGEN Redwood City, CA, USA, http://www.qiagen.com/ingenuity). This software comprises curated information from databases of experimental and predictive origin, enabling discovery of highly represented functions, pathways, and interactome networks.

Gel electrophoresis and immunoblotting

Brain samples were homogenized in RIPA lysis buffer (50 mM Tris/HCl buffer, pH 7.4 containing 2 mM EDTA, 0.2% Nonidet P-40, 1 mM PMSF, protease, and phosphatase inhibitor cocktails, Roche Molecular Systems, Basel, Switzerland). The homogenates were centrifuged for 15 min at 13,000 rpm. Protein concentrations were determined with the BCA method (Thermo Fisher). Equal amounts of protein (12 μg) for each sample were loaded and separated by electrophoresis on sodium dodecyl sulfate polyacrylamide gel electrophoresis (SDS-PAGE) (10%) gels and transferred onto nitrocellulose membranes (Amersham, Freiburg, Germany). Non-specific bindings were blocked by incubation in 3% albumin in PBS containing 0.2% Tween for 1 h at room temperature. After washing, membranes were incubated overnight at 4°C with the antibody against C9orf72 (rabbit polyclonal used at a dilution of 1:1,000; ab183982, Abcam, Cambridge, UK), TDP43-T (rabbit polyclonal used at dilution of 1:250; ab154047, Abcam), SNAP25 (mouse monoclonal used at dilution of 1:1000, SMI81, BioLegend, San Diego, CA, USA), CAMMKIIa (mouse monoclonal diluted 1:1,000; 13-7300, Zymed, MA, USA) and CAMMKIV (mouse monoclonal diluted 1:1,000; c28420, BD Biosciences, NJ, USA). Protein loading was monitored using an antibody against β-actin (mouse monoclonal diluted 1:30,000; A5316, Sigma, St. Louis, MO, USA). Membranes were then incubated for 1h in the appropriate HRP-conjugated secondary antibody (1:2,000 Agilent), and immunocomplexes were revealed by chemiluminescence reagent (ECL, Freiburg, Germany). Densitometric quantification was carried out with ImageLab software (Biorad). Bands were normalized to β-actin. Seven cases per group were analyzed.

Statistical analysis

The normality of distribution of fold change values was analyzed with the Kolmogorov-Smirnov test. The non-parametric Mann-Whitney test was performed to compare each group when values

did not follow a normal distribution, whereas the unpaired *t*-test was used for normal variables. Statistical analysis and graphic design were performed with GraphPad Prism version 5.01 (La Jolla, CA, USA). Outliers were detected using the GraphPad software QuickCalcs ($p < 0.05$). The data were expressed as mean ± SEM, and significance levels were set at $^{*}p < 0.05$, $^{**}p < 0.01$, $^{***}p < 0.001$.

RESULTS

Microarray analysis

Cofactors age, gender, RIN value, and postmortem delay were not relevant for the analysis. After filtering, 4,851 genes were included in the analysis. Gene expression in control and c9FTLD cases, with *p*-values equal to or lower than 0.05 and absolute fold change logarithm equal to or greater than 0.5, is represented in a heat-map (Fig. 1A). Forty-eight genes were differentially expressed in frontal cortex area 8 of c9FTLD when compared with controls (11 upregulated, 37 downregulated). Using GO database, we identified clusters of deregulated genes related to DNA recombination, RNA splicing regulation, RNA polymerase transcription, and centriole (Fig. 1B). Deregulated genes are listed in Table 3. In addition to reported clusters, genes linked to myelin synthesis, calcium regulation, and ubiquitin-protesome system were also deregulated. Microarray details: https://www.ebi.ac.uk/arrayexpress/; reference number fgsubs #218580.

Gene validation

Aberrant accumulation of hyper-phosphorylated TDP43 and toxic aggregates of C9orf72 are common hallmarks in c9FTLD. mRNA levels of *TARDBP and C9ORF72* were evaluated with RT-qPCR. *C9ORF72* mRNA expression was significantly decreased in c9FTLD when compared with controls ($p = 0.003$), in line with the results of the array

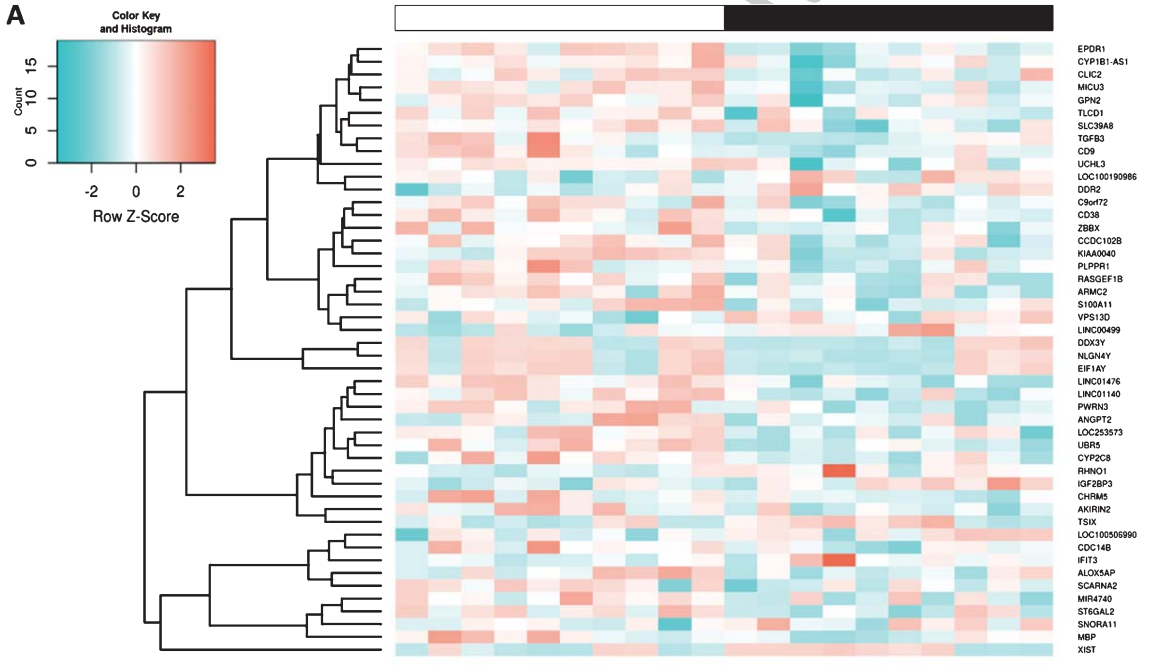

B

GO Term	Count	Size	Genes	Odds ratio	p-value
DNA recombination	7	36	H2AFX, PSMC3IP, RHNO1, RMI1, SFR1, TFRC, XRCC4	3.63	0.006660
regulation of RNA splicing	5	21	AGGF1, CELF6, CLK2, RBM10, SRSF5	4.67	0.008800
centriole	5	20	CEP290, CEP41, IFT88, POC5, TUBD1	4.99	0.00707
RNA polymerase II transcriptio	5	21	ERCC2, GTF2H3, MED14, STAT3, TAF4B	4.67	0.00808

Fig. 1. Microarray analysis. A) Hierarchical clustering heat-map of expression intensities of mRNA array transcripts in frontal cortex area 8 in c9FTLD compared with controls. B) GO database identifies clusters of deregulated genes in c9FTLD. Genes differentially expressed show an absolute fold change >2.0 in combination with a *p*-value ≤ 0.05.

Table 3
Deregulated genes in FC of c9FTLD cases

Gene ID	Coding protein	Deregulation	*FC*	*p*
NLGN4Y	Neuroligin 4 Y-Linked	Down	–1.66	0.016
DDX3Y	DEAD-Box Helicase 3 Y-Linked	Down	–1.42	0.040
EIF1AY	Eukaryotic Translation Initiation Factor 1A Y-Linked	Down	–1,16	0.020
CHRM5	Cholinergic Receptor Muscarinic 5	Down	–0.90	0.010
PWRN3	Prader-Willi Region Non-Protein Coding RNA 3	Down	–0.73	0.002
MICU3	Mitochondrial Calcium Uptake Family Member 3	Down	–0.73	0.002
MBP	Myelin Basic Protein	Down	–0.68	0.044
PLPPR1	Phospholipid Phosphatase Related 1	Down	–0.70	0.043
CD38	CD38 Molecule	Down	–0.64	0.005
LINC01476	Long Intergenic Non-Protein Coding RNA 1476	Down	–0.60	0.001
C9orf72	Chromosome 9 Open Reading Frame 72	Down	–0.60	0.006
UBR5	Ubiquitin Protein Ligase E3 Component N-Recognin 5	Down	–0.60	0.000
KIAA0040	Uncharacterized Protein KIAA0040	Down	–0,60	0.029
ALOX5AP	Arachidonate 5-Lipoxygenase Activating Protein	Down	–0.59	0.032
TGFB3	Transforming Growth Factor Beta 3	Down	–0.59	0.030
CD9	CD9 Molecule	Down	–0.58	0.048
CCDC102B	Coiled-Coil Domain Containing 102B	Down	–0.57	0.011
LOC253573	Uncharacterized LOC253573	Down	–0.57	0.005
EPDR1	Ependymin Related 1	Down	–0.57	0.001
ZBBX	Zinc Finger B-Box Domain Containing	Down	–0.57	0.040
CYP2C8	Cytochrome P450 Family 2 Subfamily C Member 8	Down	–0.57	0.015
CLIC2	Chloride Intracellular Channel 2	Down	–0.56	0.015
ST6GAL2	ST6 Beta-Galactoside Alpha-2,6-Sialyltransferase 2	Down	–0.56	0.024
RASGEF1B	RasGEF Domain Family Member 1B	Down	–0.54	0.030
MIR4740	Hsa-Mir-4740	Down	–0.53	0.034
ANGPT2	Angiopoietin 2	Down	–0.53	0.027
S100A11	S100 Calcium Binding Protein A11	Down	–0.53	0.036
UCHL3	Ubiquitin C-Terminal Hydrolase L3	Down	–0.53	0.027
TLCD1	Calfacilitin	Down	–0.52	0.024
ARMC2	Armadillo Repeat Containing 2	Down	–0.52	0.014
CYP1B1-AS1	CYP1B1 Antisense RNA 1 (Non-Protein Coding)	Down	–0.52	0.024
LINC01140	Long Intergenic Non-Protein Coding RNA 1140	Down	–0.52	0.004
GPN2	GPN-Loop GTPase 2	Down	–0.52	0.015
AKIRIN2	Akirin 2	Down	–0.52	0.007
SLC39A8	Solute Carrier Family 39 (Metal Ion Transporter), Member 8	Down	–0.51	0.031
SCARNA2	Small Cajal Body-Specific RNA 2	Down	–0.50	0.027
CDC14B	Cell Division Cycle 14B	Down	–0.50	0.044
LOC100506990	Uncharacterized LOC100506990	Up	0.51	0.036
VPS13D	Vacuolar Protein Sorting 13 Homolog D	Up	0.51	0.016
LINC00499	Long Intergenic Non-Protein Coding RNA 499	Up	0.52	0.011
DDR2	Discoidin Domain Receptor Tyrosine Kinase 2	Up	0.54	0.017
RHNO1	RAD9-HUS1-RAD1 Interacting Nuclear Orphan 1	Up	0.55	0.018
IFIT3	Interferon Induced Protein With Tetratricopeptide Repeats 3	Up	0.55	0.034
IGF2BP3	Insulin-like Growth Factor 2 MRNA Binding Protein 3	Up	0.55	0.024
LOC100190986	Uncharacterized LOC100190986	Up	0.56	0.034
SNORA11	Small Nucleolar RNA, H/ACA Box 11	Up	0.57	0.048
TSIX	TSIX Transcript, XIST Antisense RNA	Up	0.67	0.021
XIST	X Inactive Specific Transcript	Up	2.22	0.043

(Fig. 2A). *TARDBP* mRNA levels were not significant altered in c9FTLD when compared with controls ($p = 0.15$).

Significant increase in *UBR5* ($p = 0.03$) and *DD3XY* ($p = 0.026$) mRNAs was confirmed by RT-qPCR. Expression levels of *SCARNA2* ($p = 0.83$), *EIF1AY* ($p = 0.36$), and *GPN2* ($p = 0.76$), although reduced in the array, were preserved when assessed with RT-qPCR (Fig. 2B).

MBP mRNA expression was significantly decreased in c9FTLD ($p = 0.05$) (Fig. 2C). To further extend knowledge about genes linked to myelin and oligodendrocytes, RT-qPCR revealed reduced expression of *MAG* ($p = 0.036$), *MAL* ($p = 0.02$), *MOBP* ($p = 0.025$), and *MOG* ($p = 0.05$) in c9FTLD when compared with controls (Fig. 2C). However, the expression of *OLIG1* ($p = 0.17$), *OLIG2* ($p = 0.40$), *SOX10* ($p = 0.33$), *NG2* ($p = 0.34$), *MYRF*

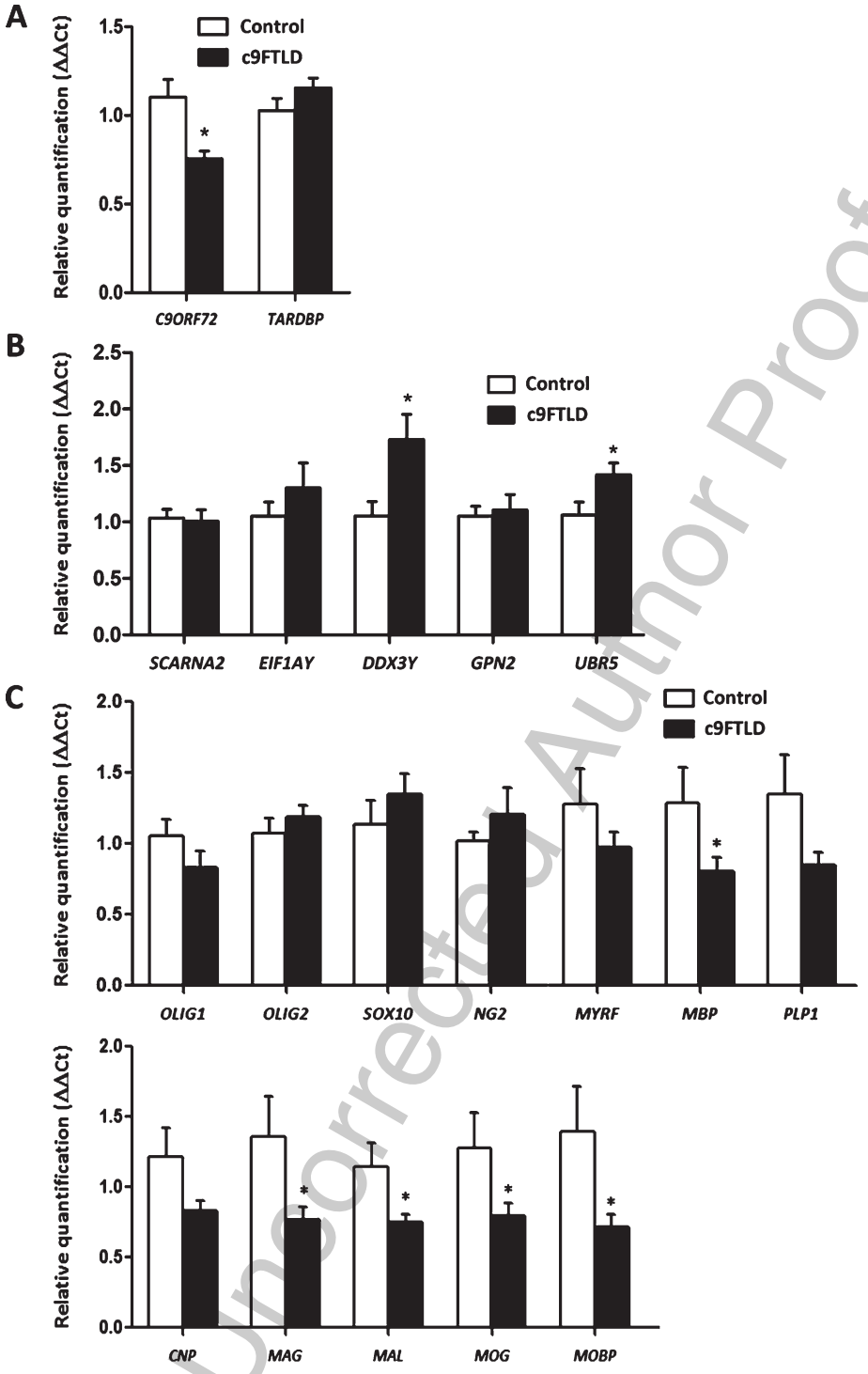

Fig. 2. mRNA expression of selected genes in c9FTLD. A) Expression levels of genes *C9ORF72* and *TARDBP*. B) Relative expression levels of genes linked to DNA/RNA regulation mechanisms. C) Expression levels of genes coding for myelin and oligodendrocyte proteins. The significance level is set at $^{*}p < 0.05$.

($p = 0.23$), *CNP* ($p = 0.065$), and *PLP1* ($p = 0.07$) was not altered in c9FTLD (Fig. 2C). None of these genes, excepting *MBP*, was identified as deregulated in the arrays.

Cortical proteostatic impairment in c9FTLD

To probe additional molecular disturbances in frontal cortex (area 8) from c9FTLD cases with respect to neurologically intact controls, a label-free MS-based approach was used. Postmortem delay was not relevant for the study. Among 3,909 identified proteins, the differential frontal cortex site-specific proteomic signature was composed of 130 proteins (40 downregulated and 90 upregulated) in c9FTLD cases when compared with controls. A heat-map representing the fold-change of identified proteins with associated *p*-values from the pair-wise quantitative comparisons, and a Volcano plot showing the distribution of differentially expressed proteins in c9FTLD and controls, are depicted in Fig. 3. Deregulated proteins are listed in Table 4.

Cortical deregulated pathways in c9FTLD

To enhance the analytical outcome of proteomic experiments, differential proteome datasets were functionally analyzed across specific biological functions using IPA software. Bioinformatic analysis revealed clusters categorized under the terms apoptosis, inflammation, metabolism of amino acids, metabolism of carbohydrates, metabolism of membrane lipid derivatives, microtubule dynamics, morphology of mitochondria, neuritogenesis, neurotransmission, phagocytosis, receptor-mediated endocytosis, and synthesis of reactive oxygen species as altered pathways in c9FTLD (Table 5). Additional integrative network unveiled disruptions in calcium signalling (NECAB1, CAMMKK2 and CNTN2), calmodulin function, and vesicle release (CLSTN1) (Fig. 4 and Table 4). Moreover, the protein interactome map showed deregulation of cross-linkers between DNA/RNA regulation systems and ubiquitin-proteasome systems, suggesting an imbalance in cellular transcription processes and protein degradation mechanisms in c9FTLD (Fig. 4).

Monitoring the frontal cortical expression of specific protein mediators in c9FTLD

In order to partially validate the results obtained by LC-MS/MS, western-blotting was used as an orthogonal technique. To complement our study, total TDP43 protein levels were increased in c9FTLD when compared with controls ($p = 0.02$). C9orf72 long isoform was significantly reduced ($p = 0.04$) whereas C9orf72 short isoform was significantly increased ($p = 0.000$) in c9FTLD (Fig. 5). In

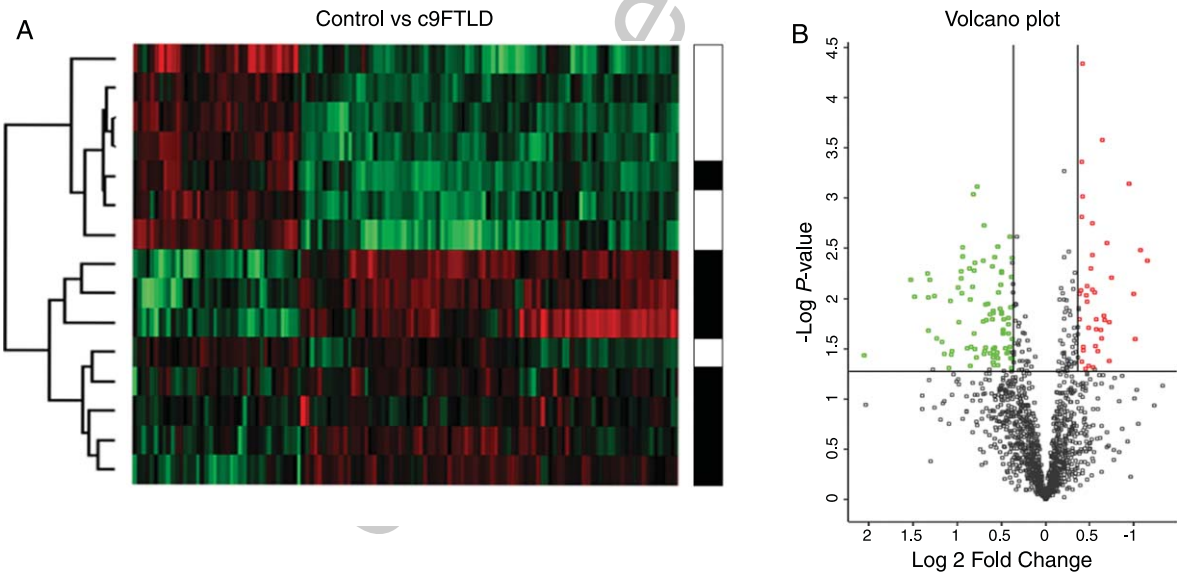

Fig. 3. Differentially expressed proteins in frontal cortex area 8 in c9FTLD. A) Heat map representing the fold-change of identified proteins with associated *p*-values from the pair-wise quantitative comparisons with controls. Significantly upregulated proteins in c9FTLD between pair-wise comparisons are labelled in green, and significantly downregulated proteins are labelled in red. B) Volcano plot of differentially expressed proteins.

Table 4
Deregulated proteins in c9FTLD compared with controls

Gene	Protein name	Uniprot	Deregulation	FC	*p*
RAP1GAP	Rap1 GTPase-activating protein 1	X6R8W7	Down	0.77	0.01
CLIP2	CAP-Gly domain-containing linker protein 2	Q9UDT6	Down	0.77	0.02
SUGT1	Protein SGT1 homolog	Q9Y2Z0	Down	0.76	0.00
AAK1	AP2-associated protein kinase 1	Q2M2I8	Down	0.76	0.01
DYNC1LI1	Cytoplasmic dynein 1 light intermediate chain 1	Q9Y6G9	Down	0.76	0.00
PRKCB	Protein kinase C beta type	P05771	Down	0.75	0.00
PRKCG	Protein kinase C gamma type	P05129	Down	0.75	0.04
CLTC	Clathrin heavy chain 1	Q00610	Down	0.75	0.00
GAS7	Growth arrest-specific protein 7	O60861	Down	0.74	0.03
NPTX1	Neuronal pentraxin-1	Q15818	Down	0.74	0.03
ARHGEF2	Rho guanine nucleotide exchange factor 2	Q92974	Down	0.73	0.05
INA	Internexin Neuronal Intermediate Filament Protein Alpha	Q16352	Down	0.73	0.01
PUF60	Poly(U)-binding-splicing factor PUF60	Q9UHX1	Down	0.72	0.01
ATL1	Atlastin-1	Q8WXF7	Down	0.72	0.01
CNTN2	Contactin-2	A0A1W2PQ11	Down	0.72	0.02
GLTP	Glycolipid transfer protein	Q9NZD2	Down	0.71	0.05
PRRT2	Proline-rich transmembrane protein 2	Q7Z6L0	Down	0.70	0.00
AIDA	Axin interactor, dorsalization-associated protein	Q96BJ3	Down	0.69	0.00
CCDC6	Coiled-coil domain-containing protein 6	Q16204	Down	0.69	0.00
NCKIPSD	NCK-interacting protein with SH3 domain	Q9NZQ3	Down	0.69	0.05
PLD3	Phospholipase D3	Q8IV08	Down	0.69	0.01
RABL6	Rab-like protein 6	Q3YEC7	Down	0.68	0.01
INF2	Inverted formin-2	Q27J81	Down	0.68	0.03
AGL	Glycogen debranching enzyme	P35573	Down	0.67	0.03
APOE	Apolipoprotein E	P02649	Down	0.67	0.02
CAMKK2	Calcium/calmodulin-dependent protein kinase kinase 2	Q96RR4	Down	0.67	0.02
GPRIN1	G protein-regulated inducer of neurite outgrowth 1	Q7Z2K8	Down	0.65	0.02
OPTN	Optineurin	Q96CV9	Down	0.65	0.02
POR	NADPH—cytochrome P450 reductase	P16435	Down	0.64	0.00
ABLIM2	Actin-binding LIM protein 2	Q6H8Q1	Down	0.63	0.02
NECAB1	N-terminal EF-hand calcium-binding protein 1	Q8N987	Down	0.63	0.01
UGGT1	UDP-glucose:glycoprotein glucosyltransferase 1	Q9NYU2	Down	0.62	0.00
STRN4	Striatin-4	Q9NRL3	Down	0.61	0.04
DNAJC11	DnaJ homolog subfamily C member 11	Q9NVH1	Down	0.61	0.02
CLSTN1	Calsyntenin-1	O94985	Down	0.59	0.01
BAG6	Large proline-rich protein BAG6	P46379	Down	0.52	0.00
SLC2A3	Solute carrier family 2, facilitated glucose transporter member 3	P11169	Down	0.50	0.01
SEC24B	Protein transport protein Sec24B	O95487	Down	0.49	0.03
ANK3	Ankyrin-3	Q12955	Down	0.47	0.00
WDR47	WD repeat-containing protein 47	O94967	Down	0.45	0.00
CPNE1	Copine-1	Q99829	Up	1.30	0.03
GAPDH	Glyceraldehyde-3-phosphate dehydrogenase	P04406	Up	1.30	0.00
PHB	Prohibitin	P35232	Up	1.30	0.04
ADH5	Alcohol dehydrogenase class-3	P11766	Up	1.31	0.04
IDH1	Isocitrate dehydrogenase [NADP] cytoplasmic	O75874	Up	1.31	0.01
MSN	Moesin	P26038	Up	1.31	0.05
CNDP2	Cytosolic non-specific dipeptidase	Q96KP4	Up	1.32	0.01
ACAA2	3-ketoacyl-CoA thiolase, mitochondrial	P42765	Up	1.33	0.00
PSMA6	Proteasome subunit alpha type-6	P60900	Up	1.33	0.03
HPX	Hemopexin	P02790	Up	1.34	0.02
PSMA4	Proteasome subunit alpha type-4	P25789	Up	1.34	0.03
SERPINB6	Serpin B6	P35237	Up	1.34	0.02
TARDBP	TAR DNA-binding protein 43	Q13148	Up	1.34	0.02
BRSK1	Serine/threonine-protein kinase BRSK1	Q8TDC3	Up	1.36	0.03
ECH1	Delta(3,5)-Delta(2,4)-dienoyl-CoA isomerase, mitochondrial	Q13011	Up	1.37	0.03
PACSIN2	Protein kinase C and casein kinase substrate in neurons protein 2	Q9UNF0	Up	1.38	0.02
PPT1	Palmitoyl-protein thioesterase 1	P50897	Up	1.39	0.02
RAB7A	Ras-related protein Rab-7a	P51149	Up	1.40	0.02
REPS1	RalBP1-associated Eps domain-containing protein 1	Q96D71	Up	1.40	0.02
ALDH9A1	4-trimethylaminobutyraldehyde dehydrogenase	P49189	Up	1.41	0.01

(*Continued*)

Table 4
(*continued*)

Gene	Protein name	Uniprot	Deregulation	FC	*p*
COPS2	COP9 signalosome complex subunit 2	P61201	Up	1.41	0.01
ECI2	Enoyl-CoA delta isomerase 2, mitochondrial	O75521	Up	1.41	0.01
EEF1A1	Elongation factor 1-alpha 1	P68104	Up	1.41	0.01
FHL1	Four and a half LIM domains protein 1 (Fragment)	Q5JXI8	Up	1.42	0.01
MPI	Mannose-6-phosphate isomerase	P34949	Up	1.43	0.01
CTSD	Cathepsin D	P07339	Up	1.45	0.01
CUTA	Protein CutA	O60888	Up	1.45	0.05
LHPP	Phospholysine phosphohistidine inorganic pyrophosphate phosphatase	Q9H008	Up	1.45	0.00
CSRP1	Cysteine and glycine-rich protein 1	P21291	Up	1.46	0.04
NUDT21	Cleavage and polyadenylation specificity factor subunit 5	O43809	Up	1.46	0.03
CLIC4	Chloride intracellular channel protein 4	Q9Y696	Up	1.47	0.04
LMNA	Prelamin-A/C	P02545	Up	1.49	0.03
SELENBP1	Selenium-binding protein 1	Q13228	Up	1.49	0.00
MTHFD1	C-1-tetrahydrofolate synthase, cytoplasmic	P11586	Up	1.50	0.03
PNPO	Pyridoxine-5′-phosphate oxidase	Q9NVS9	Up	1.50	0.04
SKP1	S-phase kinase-associated protein 1	P63208	Up	1.50	0.05
DNPEP	Aspartyl aminopeptidase	Q9ULA0	Up	1.51	0.01
FBXO2	F-box only protein 2	Q9UK22	Up	1.51	0.01
HDHD2	Haloacid dehalogenase-like hydrolase domain-containing protein 2	Q9H0R4	Up	1.51	0.04
PEBP1	Phosphatidylethanolamine-binding protein 1	P30086	Up	1.51	0.04
SMS	Spermine synthase	P52788	Up	1.51	0.03
SRI	Sorcin	P30626	Up	1.51	0.00
PSAT1	Phosphoserine aminotransferase	Q9Y617	Up	1.52	0.02
ANXA5	Annexin A5	P08758	Up	1.54	0.03
PHGDH	D-3-phosphoglycerate dehydrogenase	O43175	Up	1.54	0.01
GSTM5	Glutathione S-transferase Mu 5	P46439	Up	1.55	0.04
PLCD1	1-phosphatidylinositol 4,5-bisphosphate phosphodiesterase delta-1	P51178	Up	1.57	0.01
HSPB1	Heat shock protein beta-1	P04792	Up	1.60	0.03
NAXD	ATP-dependent (S)-NAD(P)H-hydrate dehydratase	Q8IW45	Up	1.60	0.02
PRDX2	Peroxiredoxin-2	P32119	Up	1.60	0.01
TPPP3	Tubulin polymerization-promoting protein family member 3	Q9BW30	Up	1.61	0.03
SOD2	Superoxide dismutase [Mn], mitochondrial	P04179	Up	1.62	0.04
COPS8	COP9 signalosome complex subunit 8	Q99627	Up	1.63	0.00
CUL3	Cullin-3	A0A087WTG3	Up	1.63	0.00
CYCS	Cytochrome c	P99999	Up	1.63	0.02
PKM	Pyruvate kinase PKM	P14618	Up	1.71	0.00
TMLHE	Trimethyllysine dioxygenase, mitochondrial	Q9NVH6	Up	1.72	0.04
PSMA5	Proteasome subunit alpha type-5	P28066	Up	1.74	0.03
ARL3	ADP-ribosylation factor-like protein 3	P36405	Up	1.75	0.00
GSTP1	Glutathione S-transferase P	P09211	Up	1.75	0.02
HBA1	Hemoglobin subunit alpha	P69905	Up	1.75	0.01
CD81	CD81 antigen	P60033	Up	1.77	0.00
PRDX1	Peroxiredoxin-1	Q06830	Up	1.77	0.01
NIT2	Omega-amidase NIT2	Q9NQR4	Up	1.79	0.03
AK1	Adenylate kinase isoenzyme 1	P00568	Up	1.81	0.01
GSTM2	Glutathione S-transferase	E9PHN6	Up	1.81	0.05
AK3	GTP:AMP phosphotransferase AK3, mitochondrial	Q9UIJ7	Up	1.82	0.01
FMOD	Fibromodulin	Q06828	Up	1.85	0.03
BLVRB	Flavin reductase (NADPH)	P30043	Up	1.91	0.00
NAE1	NEDD8-activating enzyme E1 regulatory subunit	Q13564	Up	1.92	0.00
PRDX6	Peroxiredoxin-6	P30041	Up	1.93	0.01
HBB	Hemoglobin subunit beta	P68871	Up	1.94	0.01
NDUFB10	NADH dehydrogenase [ubiquinone] 1 beta subcomplex subunit 10	O96000	Up	1.94	0.01
DNAH8	Dynein heavy chain 8, axonemal	Q96JB1	Up	1.98	0.02
IGKC	Immunoglobulin kappa constant	P01834	Up	1.99	0.01
ANXA2	Annexin A2	P07355	Up	2.09	0.03
ANXA1	Annexin A1	P04083	Up	2.10	0.04
LGALS1	Galectin-1	P09382	Up	2.12	0.01
EIF3I	Eukaryotic translation initiation factor 3 subunit I	Q13347	Up	2.13	0.05
SPTBN1	Spectrin beta chain, non-erythrocytic 1	Q01082	Up	2.22	0.04

(*Continued*)

Table 4
(*continued*)

Gene	Protein name	Uniprot	Deregulation	FC	*p*
PGLS	6-phosphogluconolactonase	O95336	Up	2.26	0.03
COTL1	Coactosin-like protein	Q14019	Up	2.35	0.03
MYL6	Myosin light polypeptide 6	P60660	Up	2.39	0.01
SNPH	Syntaphilin	O15079	Up	2.48	0.01
SPR	Sepiapterin reductase	P35270	Up	2.51	0.01
HBD	Hemoglobin subunit delta	P02042	Up	2.52	0.01
PGAM2	Phosphoglycerate mutase 2	P15259	Up	2.52	0.02
IAH1	Isoamyl acetate-hydrolyzing esterase 1 homolog	Q2TAA2	Up	2.80	0.01
IGHG2	Immunoglobulin heavy constant gamma 2	P01859	Up	2.88	0.01
H2AFX	Histone H2AX	P16104	Up	4.17	0.04

Table 5
Main biofunctions of abnormally expressed proteins in frontal cortex area 8 in c9FTLD

Functional terms	*p*	Proteins
Apoptosis	0.000	PEBP1, PHGDH, PPT1, LGALS1, BAG6, PHB, SRI, PKM, CYCS, PRDX1, EIF3I, H2AFX, LMNA, SPTBN1, PRDX6, POR, GSTM5, PRKCB, CLIC4, ADH5, NAE1, PRDX2, GSTP1, CTSD, OPTN, CUL3, TARDBP, GAS7, PLCD1, EEF1A1, PUF60, SLC2A3, CLTC, NPTX1, MSN, ANXA5, ANXA2, CCDC6, ANXA1, HSPB1, SOD2, RABL6, GAPDH, APOE, SELENBP1, FMOD, PRKCG
Inflammation	0.000	PHGDH, PPT1, LGALS1, PHB, PKM, PRDX1, POR, PRDX6, CPNE1, PRKCB, PRDX2, GSTP1, CTSD, OPTN, IGKC, EEF1A1, MSN, ANXA5, HBB, ANXA1, SOD2, APOE, GAPDH, HPX, SELENBP1, COTL1, CD81
Metabolism of amino acids	0.000	PHGDH, MTHFD1, CNDP2, NIT2, PKM, IDH1, SMS
Metabolism of carbohydrate	0.000	AGL, PLCD1, EEF1A1, CLTC, PKM, ANXA1, PRDX6, MPI, PRKCB, CAMKK2, GAPDH, PRDX2, APOE, IDH1, OPTN
Metabolism of membrane lipid derivative	0.004	PRDX6, POR, PLCD1, EEF1A1, PPT1, PRKCB, PRDX2, APOE, ANXA1
Microtubule dynamics	0.000	PHGDH, CSRP1, ATL1, CLSTN1, PKM, SPTBN1, PRKCB, CAMKK2, ARL3, OPTN, CD81, GAS7, BRSK1, EEF1A1, PACSIN2, MSN, RAP1GAP, NCKIPSD, CNTN2, ANK3, HSPB1, ARHGEF2, APOE, GAPDH, GPRIN1
Morphology of mitochondria	0.003	SOD2, SNPH, GAPDH, INF2, AK1
Neuritogenesis	0.000	BRSK1, CSRP1, LGALS1, NPTX1, RAP1GAP, SNPH, CNTN2, ANK3, SPTBN1, APOE, CAMKK2, GPRIN1, GAS7, TARDBP
Neurotransmission	0.005	NPTX1, CLSTN1, PRKCB, FBXO2, SRI, SNPH, APOE, PRKCG, ANK3
Phagocytosis	0.001	RAB7A, CLTC, ANXA5, MSN, CLIC4, PRKCB, RAP1GAP, PRKCG, ANXA1
Receptor-mediated endocytosis	0.001	PACSIN2, PPT1, CLTC, REPS1, NAE1, APOE
Synthesis of reactive oxygen species	0.000	PHB, ANXA2, HBB, PRDX1, ANXA1, HSPB1, PRDX6, SOD2, PRKCB, PRDX2, APOE, IDH1, GSTP1

addition, one synaptic protein, SNAP25, and two proteins linked with the calcium/calmodulin-dependent (CaM) kinase cascade were selected for validation. SNAP25 was significantly decreased ($p = 0.02$), and CaMKII and CaMKIV protein levels were significantly reduced, in c9FTLD when compared with controls ($p = 0.05$ and $p = 0.03$, respectively) (Fig. 5).

DISCUSSION

This study analyzes differential mRNA and protein expression in frontal cortex area 8 in 19 fFTLD cases linked to C9ORF72 expansion (c9FTLD) and 14 age- and gender-matched controls using microarray hybridization and 7000G platform technology from Affymetrix® and quantitative proteomics using LC-MS/MS, respectively. mRNA expression for selected genes was validated with RT-qPCR, and protein levels with gel electrophoresis and western blotting.

Regarding TDP-43 and C9orf72, major pathologic components in c9FTLD, *TARDBP* mRNA expression was preserved but total TDP-43 protein showed increased levels in c9FTLD when compared with controls. This is in accordance with the abnormal deposition of this protein in intracellular inclusions and threads characteristic of this disease. In contrast, *C9ORF72* mRNA expression was significantly decreased in c9FTLD. However, the C9orf72 long isoform was significantly reduced and the C9orf72 short isoform significantly increased in c9FTLD. Reduced C9ORF72 protein levels were found in previous reports [55–58]. The functional implications of the reduced levels of the long C9orf72 isoform are not known, but quantitative mass spectrometry-based proteomics used to identify interacting proteins

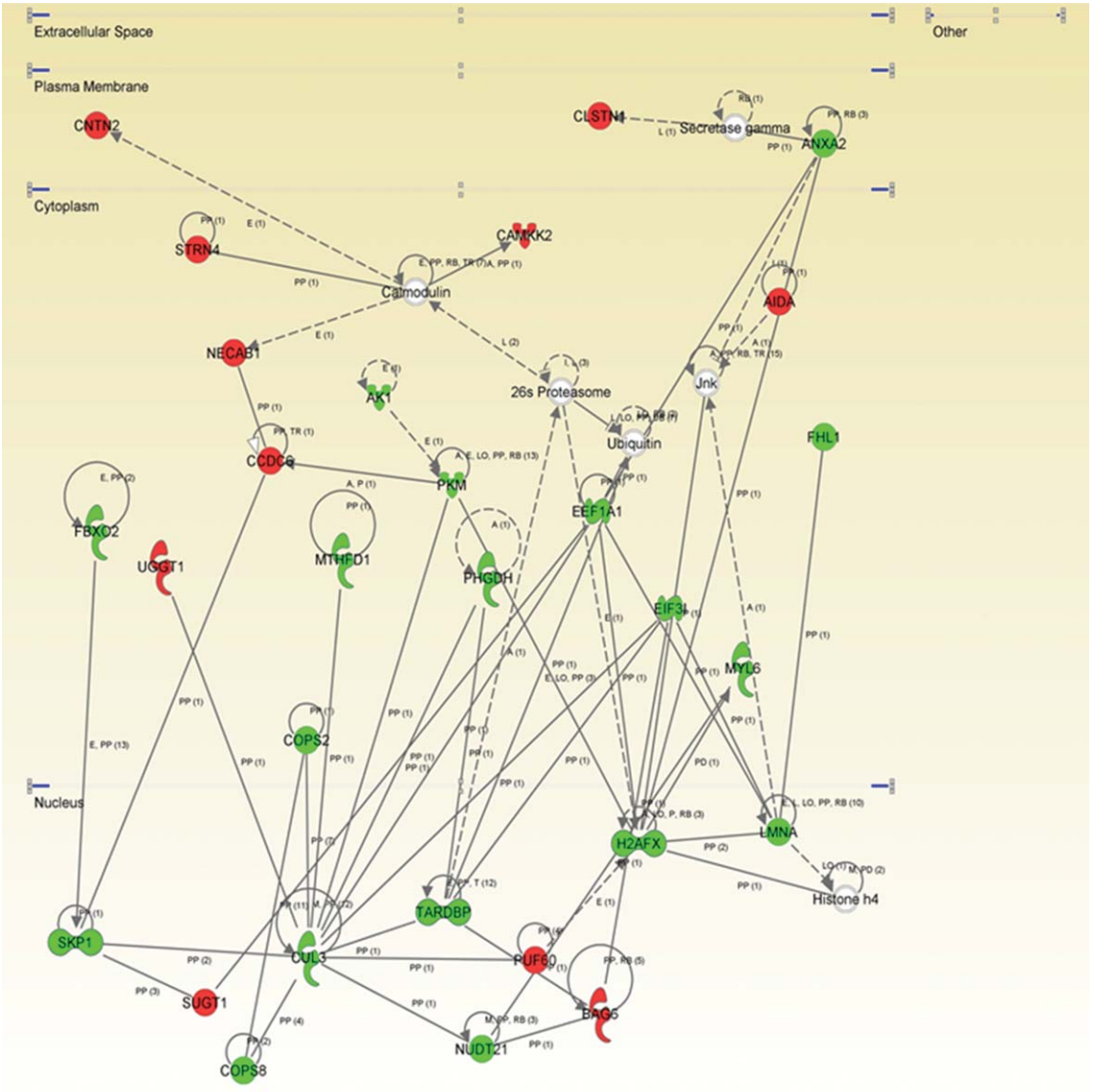

Fig. 4. High-scoring protein interactome map of differentially expressed proteins in the frontal cortex in c9FTLD. Visual representation of the relationships between differentially expressed proteins and functional interactors. Downregulated proteins are highlighted in red and upregulated proteins in green. Continuous and discontinuous lines represent direct and indirect interactions, respectively.

in motor neurons has shown that the long isoform complex stabilizes SMCR8, a protein which acts as an autophagic regulator [59, 60]. Therefore, reduced levels of the long isoform may interfere with normal autophagy and lysosomal processing [60]. C9orf72 also binds to several proteins including members of the Rab family, endoplasmic reticulum and synapses; nuclear and cytoplasmic transport, endoplasmic reticulum stress, and altered synaptic function have all been reported in association with pathogenic *C9ORF72* expansions [21, 22, 26, 28, 35, 39, 61].

The present study reveals altered gene transcription related to DNA recombination, RNA splicing regulation, RNA polymerase transcription, myelin synthesis, calcium regulation, and ubiquitin-proteasome system in c9FTLD. Proteomics performed in the same tissue samples identifies altered protein expression linked to apoptosis, inflammation, metabolism of amino acids, metabolism

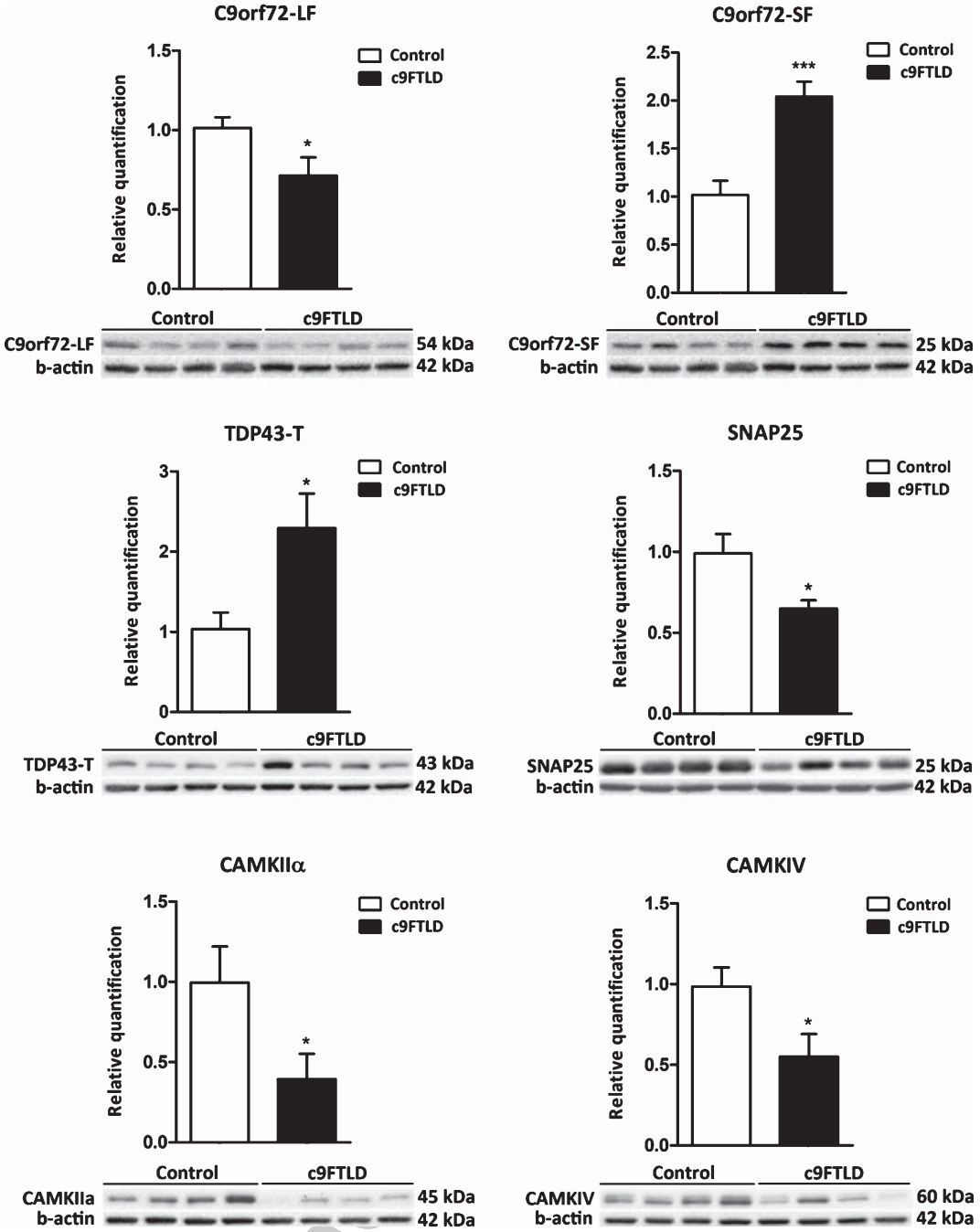

Fig. 5. Gel electrophoresis and western blotting to C9orf72 isoforms, and total TDP-43, CAMKIIa, and CAMKIV in frontal cortex area 8 in c9FTLD and controls. The protein expression of C9orf72 long isoform (54 kDa) is reduced in parallel with the increased protein level of the C9orf72 short isoform (25 kDa). Total protein levels of TDP-43 are significantly increased in c9FTLD. CAMKII and CAMKIV protein levels are significantly decreased. $^{*}p < 0.05$ and $^{***}p < 0.001$.

of carbohydrates, metabolism of membrane lipid derivatives, microtubule dynamics, morphology of mitochondria, neuritogenesis, neurotransmission, phagocytosis, receptor-mediated endocytosis, synthesis of reactive oxygen species, and calcium signaling in c9FTLD.

Genes and proteins do not match in the two lists of deregulated mRNAs and proteins in c9FTLD

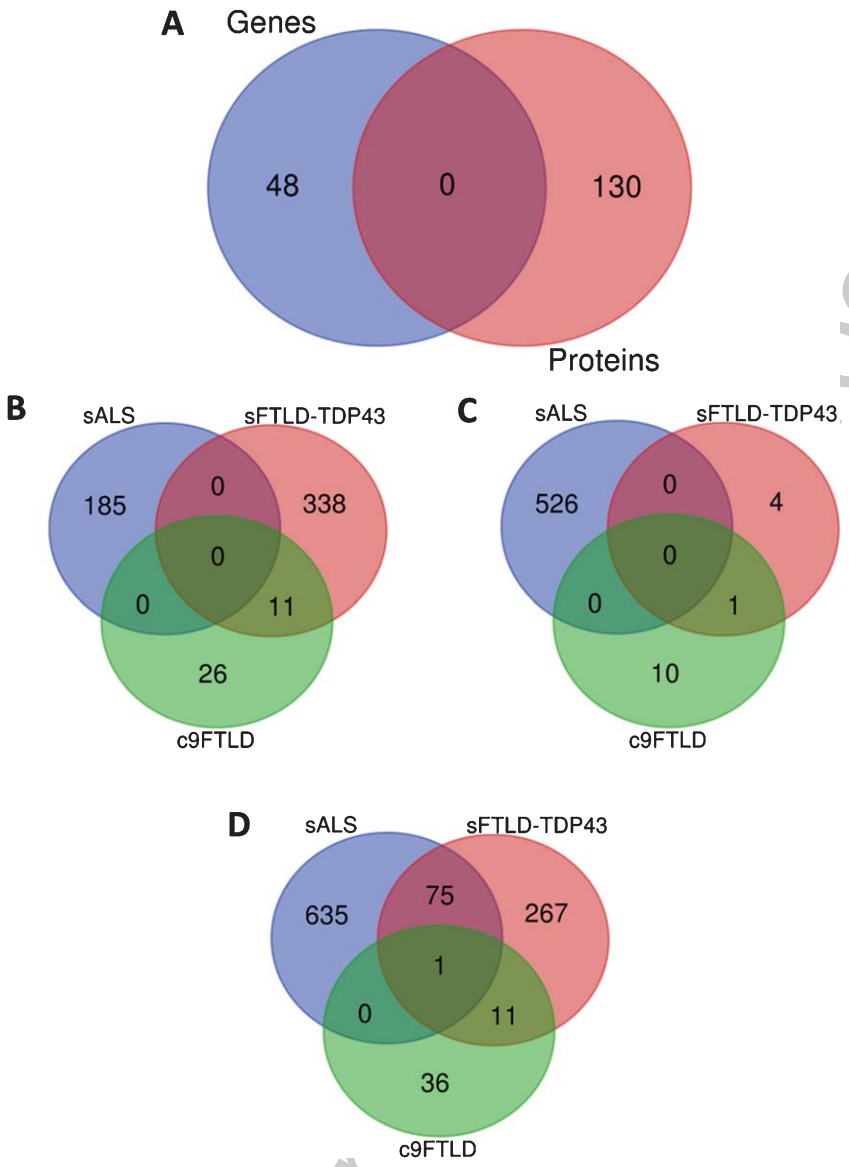

Fig. 6. A) Venn's diagram comparing transcriptomics and proteomics profile in c9FTLD based on the present observations. B–D) Overlap of the transcriptomic profiles obtained in the frontal cortex area 8 in sALS, sFTLD-TDP, and c9FTLD based on the present observations and our previous studies cited in [45] and [51]. B) Venn's diagram of downregulated genes in sALS, sFTLD, and c9FTLD. C) Venn's diagram of upregulated genes in sALS, sFTLD, and c9FTLD. D) Venn's diagram of total deregulated genes in sALS, sFTLD, and c9FTLD.

(Fig. 6A). However, a protein interactome map constructed using the IPA software shows deregulation of cross-linkers between DNA/RNA regulation systems and ubiquitin-proteasome systems, suggesting an imbalance in cellular transcription processes and protein degradation mechanisms, which makes sense in light of gene transcription observations of the main contributors to the pathogenesis of neurodegenerative diseases with abnormal protein aggregates, and it is particularly in line with the function of TDP-43 and C9orf72.

Together, this combined transcriptomics-proteomics analysis supports the list of separately reported altered pathways linked to *C9ORF72* mutations, including those involved in DNA recombination and transcription, RNA splicing, endoplasmic reticulum and mitochondria, synaptic transmission, protein degradation, calcium home-

ostasis, and inflammation [35, 37–39, 41, 61–66]. Additional alterations involve altered metabolism of amino acids and carbohydrates, membrane lipid derivatives, and microtubule dynamics, and synthesis of reactive oxygen species. Links between oxidative and endoplasmic reticulum stress, TDP-43, and docosahexaenoic acid have been described in the spinal cord in ALS [67–69] but information is lacking about c9FTLD. Moreover, oxidative damage has been assessed and proven in FTLD-TDP [70], but no special focus on c9FTLD was provided in that study.

An interesting deregulated cluster is composed of genes linked to several miRNAs, nuclear RNAs and long non-coding RNAs, including MIR4740, the small nucleolar RNA (SCARNA2), and long non-coding RNAs such as X-inactive specific transcript (XIST) and the long intergenic non-coding RNAs LINC1476, LINC1140, and LINC00499. miRNAS participate in a large number of variegated processes covering mRNA silencing and regulation of gene transcription [71, 72]. SCARNA2 localizes to Cajal bodies, the process of binding of its box C/D being modulated by coilin [73]. Long intergenic non-coding RNAs are mainly localized in the nucleus where they modulate chromatin and genome architecture, in addition to RNA stabilization and transcription regulation [74]. XIST is localized in the X-chromosome and participates in the inactivation of chromosome X [75]. The consequences of XIST deregulation in C9orf72 remains elusive.

Our previous studies using a similar transcriptomics approach in frontal cortex area 8 in sFTLD-TDP have shown down-deregulation of genes linked to neurotransmission and synapses, neuronal architecture, cytoskeleton of axons and dendrites, vesicle trafficking, purines, mitochondria, and energy metabolism [45]. Additional protein and enzymatic studies have revealed altered mitochondrial function and oxidative phosphorylation [45]. Using the same methods, we observed upregulated gene clusters in frontal cortex area 8 in sALS involving neurotransmission, synaptic proteins, and vesicle trafficking, and downregulated genes clustering into oligodendrocyte function and myelin-related proteins [51]. Venn's diagrams serve to illustrate downregulated and upregulated genes shared in these diseases: sALS, sFTLD-TDP, and c9FTLD (Fig. 6B–D).

Curiously, some downregulated clusters related mainly to synapses and neurotransmission in frontal cortex in sFTLD-TDP were upregulated in frontal cortex in sALS without dementia [45, 51]. The present observations in c9FTLD reveal some commonalities with sFTLD-TDP in altered clusters but not in particular genes. Downregulation of genes linked to oligodendrocytes and myelin in frontal cortex area 8 is shared in c9FTLD and sALS.

Recent studies have shown oligodendrocytes as key players in neurodegenerative diseases with abnormal protein aggregates [76]. Oligodendrogliopathy is common in sALS and FTLD-TDP. Phosphorylated-TDP-43-immunoreactive oligodendroglial inclusions are found, in addition to spinal cord motor neurons, in the motor, sensory and premotor cortex, but not in the corpus callosum, cingulum or lateral tracts of the spinal cord [77]. TDP-43 oligodendroglial inclusions are common in the deep layers of the cerebral cortex and white matter in FTLD-TDP [78]. The functional effects of oligodendroglial TDP-43 inclusions are not known, but present findings indicate altered oligodendroglial gene expression in the frontal cortex in c9FTLD. Particular features are linked to C9orf72 hexanucleotide repeat expansion [79, 80], and TDP-43-dependent or TDP-43-independent oligodendroglial dysfunction might be a characteristic trait linked to C9orf72 hexanucleotide repeat expansion.

In contrast, although astrocytes play key pathogenic roles in ALS [81], TDP-43-immunoreactive inclusions are rare in sALS and FTLD-TDP [82].

Commonalities and discrepancies are also seen when comparing the transcriptome of the frontal cortex in sALS with no mutations and ALS linked to C9orf72 mutations (c9ALS) [83]. The number and type of deregulated genes in c9ALS was approximately double that seen in sALS. For example, alteration of the unfolded protein response and intracellular protein transport were identified from genes differentially upregulated in c9ALS but not in sALS, whereas alterations in oxidative phosphorylation, cytoskeleton, and synaptic transmission were predominant in frontal cortex in sALS [83]. These data in frontal cortex in sALS roughly correlate with our observations in the sALS/sFTLD-TDP spectrum [45, 51] although the lack of information regarding the cognitive status of patients in the c9ALS/sALS comparative study does not permit further analogies between the separate series. That study was performed using RNA-sequencing methods [83], which uses high-throughput sequencing to document all transcripts in contrast to microarrays which quantify a set of predetermined sequences. Therefore, RNA-seq is presumably more robust than our microarrays

approach, and may account for differences in the results obtained by these different strategies. However, focusing on c9ALS and present observations in c9FTLD, altered RNA splicing and ubiquitin-proteasome system are identified in both studies.

Comparisons with other studies performed in different types of FTLD-TDP show disparate results. One gene expression analysis in fFTLD linked to *GRN* mutations identified abnormal regulated processes associated with lipid metabolism, MAPK signaling pathway, and transport [43], while lysosomal dysfunction was identified in another [44]. Another study recognized synapse-, cytoskeletal/filament-, microtubule/axon-, and proteasome-related pathways in FTLD-TDP when compared with controls, and cytoskeletal protein-, mitochondria/energy-, synapse-, microtubule/axon-, and ubiquitin-proteasome-associated deregulation when comparing FTLD-TDP with FTLD associated with motor neuron disease [42]. Common mechanisms occur within the FTLD-ALS spectrum [84]. However, weighted co-expression network proteomic analysis has recently revealed 15 modules of co-expressed proteins, eight of which differed significantly across the ALS-FTD disease spectrum [46]. Interestingly, a module enriched with astrocyte and microglia proteins was significantly increased in the frontal cortex in ALS cases carrying the C9orf72 mutation compared to sporadic ALS cases, suggesting that the genetic expansion is associated with inflammation in the brain [46]. Increased levels of proteins linked to inflammation are also identified in the frontal cortex in C9orf72 in our study. The present dual-omic approach, like the majority of molecular studies carried out in the postmortem human brain, is based on the relative abundance of particular mRNAs and proteins or ratios of two absolute concentrations (fold-change) representing concentrations relative to reference samples. Moreover, the agonal state and postmortem delay may differentially interfere with transcription and protein synthesis/degradation. Therefore, when analyzing postmortem brain samples, a non-steady-state condition is always the real scenario. This statement is important when assessing transcripts and proteins separately, but it is especially crucial when analyzing RNA and protein correlations of particular genes in human postmortem brain [85–87]. Moreover, distinct cell populations are usually mingled, and rates and scales of RNA and corresponding encoded proteins may be cell type-dependent. These facts, together with particular characteristics of samples, and differences in the procedures and methods, may account for the non-homogeneous results in different laboratories. Although the original samples are the same in the present series, and the identified altered pathways are similar and complementary using a combination of transcriptomics and proteomics, it is worth stressing that different RNAs and proteins are identified by these methods. Combined non-targeted '-omics' seems to be a valuable approach to deciphering altered molecular pathways in FTLD provided that observations are viewed cautiously when assessing human postmortem brain samples.

ACKNOWLEDGMENTS

We wish to thank Valle de Hebron Institute of Research (VHIR) Whole-transcriptome array platform for their help in the arrays, and T. Yohannan for editorial assistance.

This study was supported by grants from CIBERNED and PI17/00809 Institute of Health Carlos III, and co-funded by FEDER funds/European Regional Development Fund (ERDF) – a way to build Europe; ALS intra-CIBERNED project to IF; IFI15/00035 fellowship to PA-B; "Retos todos unidos contra la ELA" and "Proyecto DGeneración conexiones con sentido" to MP; and grant from the "Fundación Tatiana Pérez de Guzmán el Bueno, convocatoria Neurociencias 2014" to EG. Additional support came from grants from the Department of Economic Development of the Government of Navarra (Ref. PC025, PC081-82) to ES. The Proteomics Unit of Navarrabiomed is a member of Proteored, PRB3-ISCIII, and is supported by grant PT17/0019, of the PE I+D+i 2013-2016 to JFI, funded by ISCIII and ERDF.

Authors' disclosures available online (https://www.j-alz.com/manuscript-disclosures/18-1123r2).

SUPPLEMENTARY MATERIAL

The supplementary material is available in the electronic version of this article: http://dx.doi.org/10.3233/JAD-181123.

REFERENCES

[1] Hortobagyi T, Cairns NJ (2015) Amyotrophic lateral sclerosis and frontotemporal lobar degeneration. In *Neuropathology of neurodegenerative diseases: A practical guide*, Kovacs GG, ed. Cambridge University Press, Cambridge, pp. 209-248.

[2] Lashley T, Roher JD, Mead S, Revesz T (2015) Review: An update on clinical, genetic and pathological aspects of frontotemporal lobar degenerations. *Neuropathol Appl Neurobiol* **41**, 858-881.

[3] Mann DMA, Snowden JS (2017) Frontotemporal lobar degeneration: Pathogenesis, pathology and pathways to phenotype. *Brain Pathol* **27**, 723-736.

[4] Van Mossevelde S, Engelborghs S, van der Zee J, Broeckhoven C (2018) Genotype-phenotype links in frontotemporal lobar degeneration. *Nature Rev Neurol* **14**, 363-378.

[5] Olszewska DA, Lonergan R, Fallon EM, Lynch T (2016) Genetics of frontotemporal dementia. *Curr Neurol Neurosci Rep* **16**, 107.

[6] Pottier C, Ravenscroft TA, Sánchez-Contreras M, Rademakers R (2016) Genetics of FTLD: Overview and what else we can expect from genetic studies. *J Neurochem* **138**, 32-53.

[7] Rainero I, Rubino E, Michelerio A, D'Agata F, Gentile S, Pinessi L (2017) Recent advances in the molecular genetics of frontotemporal lobar degeneration. *Funct Neurol* **32**, 7-16.

[8] Neumann M, Mackenzie IRA (2019) Neuropathology of non-tau frontotemporal lobar degeneration. *Neuropathol Appl Neurobiol* **45**, 19-40.

[9] Neumann M, Sampathu DM, Kwong LK, Truax AC, Micsenyi MC, Chou TT, Bruce J, Schuck T, Grossman M, Clark CM, McCluskey LF, Miller BL, Masliah E, Mackenzie IR, Feldman H, Feiden W, Kretzschmar HA, Trojanowski JQ, Lee VM (2006) Ubiquitinated TDP-43 in frontotemporal lobar degeneration and amyotrophic lateral sclerosis. *Science* **314**, 130-133.

[10] Geser F, Martinez-Lage M, Robinson J, Uryu K, Neumann M, Brandmeir NJ, Xie SX, Kwong LK, Elman L, McCluskey L, Clark CM, Malunda J, Miller BL, Zimmerman EA, Qian J, Van Deerlin V, Grossman M, Lee VM, Trojanowski JQ (2009) Clinical and pathological continuum of multisystem TDP-43 proteinopathies. *Arch Neurol* **66**, 180-189.

[11] DeJesús-Hernández M, Mackenzie IR, Boeve BF, Boxer AL, Baker M, Rutherford NJ, Nicholson AM, Finch NA, Flynn H, Adamson J, Kouri N, Wojtas A, Sengdy P, Hsiung GY, Karydas A, Seeley WW, Josephs KA, Coppola G, Geschwind DH, Wszolek ZK, Feldman H, Knopman DS, Petersen RC, Miller BL, Dickson DW, Boylan KB, Graff-Radford NR, Rademakers R (2011) Expanded GGG GCC hexanucleotide repeat in non-coding region of C9ORF72 causes chromosome 9p-linked FTD and ALS. *Neuron* **72**, 245-256.

[12] Cruts M, Gijselinck I, Van Langenhove T, Van der Zee J, Van Broeckhoven C (2013) Current insights into the C9orf72 repeat expansion diseases of the FTLD/ALS spectrum. *Trends Neurosci* **36**, 450-499.

[13] Renton AE, Chiò A, Traynor BJ (2014) State of play in amyotrophic lateral sclerosis genetics. *Nat Neurosci* **17**, 17-23.

[14] Stewart H, Rutherford NJ, Briemberg H, Krieger C, Cashman N, Fabros M, Baker M, Fok A, DeJesús-Hernández M, Eisen A, Rademakers R, Mackenzie IR (2012) Clinical and pathological features of amyotrophic lateral sclerosis caused by mutation in the C9ORF72 gene on chromosome 9p. *Acta Neuropathol* **123**, 409-417.

[15] Boeve BF, Boylan KB, Graff-Radford NR, DeJesus-Hernandez M, Knopman DS, Pedraza O, Vemuri P, Jones D, Lowe V, Murray ME, Dickson DW, Josephs KA, Rush BK, Machulda MM, Fields JA, Ferman TJ, Baker M, Rutherford NJ, Adamson J, Wszolek ZK, Adeli A, Savica R, Boot B, Kuntz KM, Gavrilova R, Reeves A, Whitwell J, Kantarci K, Jack CR Jr, Parisi JE, Lucas JA, Petersen RC, Rademakers R (2012) Characterization of frontotemporal dementia GCC repeat expansion in C9ORF72. *Brain* **135**, 765-783.

[16] Gendron TF, Bieniek KF, Zhang YJ, Jansen-West K, Ash PE, Caulfield T, Daughrity L, Dunmore JH, Castanedes-Casey M, Chew J, Cosio DM, van Blitterswijk M, Lee WC, Rademakers R, Boylan KB, Dickson DW, Petrucelli L (2013) Antisense transcripts of the expanded C9ORF72 hexanucleotide repeat form nuclear RNA foci and undergo repeat-associated non-ATG translation in c9FTD/ALS. *Acta Neuropathol* **126**, 829-844.

[17] Lee YB, Chen HJ, Peres JN, Gomez-Deza J, Attig J, Stalekar M, Troakes C, Nishimura AL, Scotter EL, Vance C, Adachi Y, Sardone V, Miller JW, Smith BN, Gallo JM, Ule J, Hirth F, Rogelj B, Houart C, Shaw CE (2013) Hexanucleotide repeats in ALS/FTD form length-dependent RNA foci, sequester RNA binding proteins, and are neurotoxic. *Cell Rep* **5**, 1178-1186.

[18] Donnelly CJ, Zhang PW, Pham JT, Haeusler AR, Mistry NA, Vidensky S, Daley EL, Poth EM, Hoover B, Fines DM, Maragakis N, Tienari PJ, Petrucelli L, Traynor BJ, Wang J, Rigo F, Bennett CF, Blackshaw S, Sattler R, Rothstein JD (2013) RNA toxicity from the ALS/FTD C9ORF72 expansion is mitigated by antisense intervention. *Neuron* **80**, 415-428.

[19] Sareen D, O'Rourke JG, Meera P, Muhammad AK, Grant S, Simpkinson M, Bell S, Carmona S, Ornelas L, Sahabian A, Ornelas L, Sahabian A, Gendron T, Petrucelli L, Baughn M, Ravits J, Harms MB, Rigo F, Bennett CF, Otis TS, Svendsen CN, Baloh RH (2013) Targeting RNA foci in iPSC-derived motor neurons from ALS patients with a C9ORF72 repeat expansion. *Sci Transl Med* **5**, 208ra149.

[20] Mizielinska S, Lashley T, Norona FE, Clayton EL, Ridler CE, Fratta P, Isaacs AM (2013) C9orf72 frontotemporal lobar degeneration is characterised by frequent neuronal sense and antisense RNA foci. *Acta Neuropathol* **126**, 845-857.

[21] May S, Hornburg D, Schludi MH, Arzberger T, Rentzsch K, Schwenk BM, Grasser FA, Mori K, Kremmer E, Banzhaf-Strathmann, Mann M, Meissner F (2014) C9orf72 FTLD/ALS-associated Gly-Ala dipeptide repeat proteins cause neuronal toxicity and Unc119 sequestration. *Acta Neuropathol* **128**, 485-503.

[22] Zhang YJ, Jansen-West K, Xu YF, Gendron TF, Bieniek KF, Lin WL, Sasaguri H, Caulfield T, Hubbard J, Daughrity L, Chew J, Belzil VV, Prudencio M, Stankowski JN, Castanedes-Casey M, Whitelaw E, Ash PE, DeTure M, Rademakers R, Boylan KB, Dickson DW, Petrucelli L (2014) Aggregation-prone c9FTD/ALS poly(GA) RANtranslated proteins cause neurotoxicity by inducing ER stress. *Acta Neuropathol* **128**, 505-524.

[23] Wen X, Tan W, Westergard T, Krishnamurthy K, Markandaiah SS, Shi Y, Lin S, Shneider NA, Monaghan J, Pandey UB, Pasinelli P, Ichida JK, Trotti D (2014) Antisense proline-arginine RAN dipeptides linked to C9ORF72-ALS/FTD form toxic nuclear aggregates that initiate in vitro and in vivo neuronal death. *Neuron* **84**, 1213-1225.

[24] Cooper-Knock J, Walsh MJ, Higginbottom A, Robin Highley J, Dickman MJ, Edbauer D, Ince PG, Wharton SB, Wilson SA, Kirby J Wharton SB, Wilson SA, Kirby J, Hautbergue GM, Shaw PJ (2014) Sequestration of multi-

ple RNA recognition motif-containing proteins by C9orf72 repeat expansions. *Brain* **137**, 2040-2051.

[25] Kwon I, Xiang S, Kato M, Wu L, Theodoropoulos P, Wang T, Kim J, Yun J, Xie Y, McKnight SL (2014) Poly-dipeptides encoded by the C9orf72 repeats bind nucleoli, impede RNA biogenesis, and kill cells. *Science* **345**, 1139-1145.

[26] Freibaum BD, Lu Y, Lopez-Gonzalez R, Kim NC, Almeida S, Lee KH, Badders N, Valentine M, Miller BL, Wong PC, Petrucelli L, Kim HJ, Gao FB, Taylor JP (2015) GGG GCC repeat expansion in C9orf72 compromises nucleocytoplasmic transport. *Nature* **525**, 129-133.

[27] Tao Z, Wang H, Xia Q, Li K, Li K, Jiang X, Xu G, Wang G, Ying Z (2015) Nucleolar stress and impaired stress granule formation contribute to C9orf72 RAN translation-induced cytotoxicity. *Hum Mol Genet* **24**, 2426-2441.

[28] Jovicic A, Mertens J, Boeynaems S, Bogaert E, Chai N, Yamada SB, Paul JW 3rd, Sun S, Herdy JR, Bieri G, Kramer NJ, Gage FH, Van Den Bosch L, Robberecht W, Gitler AD (2015) Modifiers of C9orf72 dipeptide repeat toxicity connect nucleo-cytoplasmic transport defects to FTD/ALS. *Nat Neurosci* **18**, 1226-1229.

[29] Schludi MH, May S, Grasser FA, Rentzsch K, Kremmer E, Kupper C, Klopstock T, Arzberger T, German Consortium for Frontotemporal Lobar Degeneration, Bavarian Brain Banking (2015) Distribution of dipeptide repeat proteins in cellular models and C9orf72 mutation cases suggests link to transcriptional silencing. *Acta Neuropathol* **130**, 537-555.

[30] Porta S, Kwong LK, Trojanowski JQ, Lee VM (2015) Drosha inclusions are new components of dipeptide-repeat protein aggregates in FTLD-TDP and ALS C9orf72 expansion cases. *J Neuropathol Exp Neurol* **74**, 380-387.

[31] Todd TW, Petrucelli L (2016) Insights into the pathogenic mechanisms of chromosome 9 open reading frame 72 (C9orf72) repeat expansions. *J Neurochem* **138**, 145-162.

[32] Cooper-Knock J, Higginbottom A, Stopford MJ, Highley JR, Ince PG, Wharton SB, Pickering-Brown S, Kirby J, Hautbergue GM, Shaw PJ (2015) Antisense RNA foci in the motor neurons of C9ORF72-ALS patients are associated with TDP-43 proteinopathy. *Acta Neuropathol* **130**, 63-75.

[33] Xiao S, MacNair L, McLean J, McGoldrick P, McKeever P, Soleimani S, Keith J, Zinman L, Rogaeva E, Robertson J (2016) C9orf72 isoforms in amyotrophic lateral sclerosis and frontotemporal lobar degeneration. *Brain Res* **1647**, 43-49.

[34] Zhang YJ, Gendron TF, Grima JC, Sasaguri H, Jansen-West K, Xu YF, Katzman RB, Gass J, Murray ME, Shinohara M, Lin WL, Garrett A, Stankowski JN, Daughrity L, Tong J, Perkerson EA, Yue M, Chew J, Castanedes-Casey M, Kurti A, Wang ZS, Liesinger AM, Baker JD, Jiang J, Lagier-Tourenne C, Edbauer D, Cleveland DW, Rademakers R, Boylan KB, Bu G, Link CD, Dickey CA, Rothstein JD, Dickson DW, Fryer JD, Petrucelli L (2016) C9ORF72 poly(GA) aggregates sequester and impair HR23 and nucleocytoplasmic transport proteins. *Nat Neurosci* **19**, 668-677.

[35] Gao FB, Almeida S, López-González R (2017) Dysregulated molecular pathways in amyotrophic lateral sclerosis–frontotemporal dementia spectrum disorder. *EMBO J* **36**, 2931-2950.

[36] DeJesús-Hernández M, Finch NA, Wang X, Gendron TF, Bieniek KF, Heckman MG, Vasilevich A, Murray ME, Rousseau L, Weesner R, Lucido A, Parsons M, Chew J, Josephs KA, Parisi JE, Knopman DS, Petersen RC, Boeve BF, Graff-Radford NR, de Boer J, Asmann YW, Petrucelli L, Boylan KB, Dickson DW, van Blitterswijk M, Rademakers R (2017) In-depth clinico-pathological examination of RNA foci in a large cohort of C9ORF72 expansion carriers. *Acta Neuropathol* **134**, 255-269.

[37] Budini M, Buratti E, Morselli E, Criollo A (2017) Autophagy and its impact on neurodegenerative diseases: New roles for TDP-43 and C9orf72. *Front Mol Neurosci* **10**, 170.

[38] Ji YJ, Ugolino J, Brady NR, Hamacher-Brady A, Wang J (2017) Systemic deregulation of autophagy upon loss of ALS- and FTD-linked C9orf72. *Autophagy* **13**, 1254-1255.

[39] Vatsavayai SC, Nana AL, Yokoyama JS, Seeley WW (2019) C9orf72-FTD/ALS pathogenesis: Evidence from human neuropathological studies. *Acta Neuropathol* **137**, 1-26.

[40] Zhang Y, Burberry A, Wang JY, Sandoe J, Ghosh S, Udeshi ND, Svinkina T, Mordes DA, Mok J, Charlton M, Li QZ, Carr SA, Eggan K (2018) The C9orf72-interacting protein Smcr8 is a negative regulator of autoimmunity and lysosomal exocytosis. *Genes Dev* **32**, 929-943.

[41] Herrmann D, Parlato R (2018) C9orf72-associated neurodegeneration in ALS-FTD: Breaking new ground in ribosomal RNA and nucleolar dysfunction. *Cell Tissue Res* **373**, 351-360.

[42] Mishra M, Paunesku T, Woloschak GE, Siddique T, Zhu LJ, Lin S, Greco K, Bigio EH (2007) Gene expression analysis of frontotemporal lobar degeneration of the motor neuron disease type with ubiquitinated inclusions. *Acta Neuropathol* **114**, 81-94

[43] Chen-Plotkin AS, Geser F, Plotkin JB, Clark CM, Kwong LK, Yuan W, Grossman M, Van Deerlin VM, Trojanowski JQ, Lee VM (2008) Variations in the progranulin gene affect global gene expression in frontotemporal lobar degeneration. *Hum Mol Genet* **17**, 1349-1362.

[44] Evers BM, Rodríguez-Navas C, Tesla RJ, Prange-Kiel J, Wasser CR, Yoo KS, McDonald J, Cenik B, Ravenscroft TA, Plattner F, Rademakers R, Yu G, White CL 3rd, Herz J (2017) Lipidomic and transcriptomic basis of lysosomal dysfunction in progranulin deficiency. *Cell Rep* **20**, 2565-2574.

[45] Andrés-Benito P, Gelpi E, Povedano M, Santpere G, Ferrer I (2018) Gene expression profile in frontal cortex in sporadic frontotemporal lobar degeneration-TDP. *J Neuropathol Exp Neurol* **77**, 608-627.

[46] Umoh ME, Dammer EB, Dai J, Duong DM, Lah JJ, Levey AI, Gearing M, Glass JD, Seyfried NT (2018) A proteomic network approach across the ALS-FTD disease spectrum resolves clinical phenotypes and genetic vulnerability in human brain. *EMBO Mol Med* **10**, 48-62.

[47] Mackenzie IR, Neumann M, Baborie A, Sampathu DM, Du Plessis D, Jaros E, Perry RH, Trojanowski JQ, Mann DM, Lee VM (2011) A harmonized classification system for FTLD-TDP pathology. *Acta Neuropathol* **122**, 111-113.

[48] Brettschneider J, Del Tredici K, Irwin DJ, Grossman M, Robinson JL, Toledo JB, Fang L, Van Deerlin VM, Ludolph AC, Lee VM, Braak H, Trojanowski JQ (2014) Sequential distribution of pTDP-43 pathology in behavioral variant frontotemporal dementia (bvFTD). *Acta Neuropathol* **127**, 423-439.

[49] Durrenberger PF, Fernando S, Kashefi SN, Ferrer I, Hauw JJ, Seilhean D, Smith C, Walker R, Al-Sarraj S, Troakes C, Palkovits M, Kasztner M, Huitinga I, Arzberger T, Dexter DT, Kretzschmar H, Reynolds R (2010) Effects of antemortem and postmortem variables on human brain mRNA quality: A BrainNet Europe study. *J Neuropathol Exp Neurol* **69**, 70-81.

[50] Gentleman RC, Carey VJ, Bates DM, Bolstad B, Dettling M, Dudoit S, Ellis B, Gautier L, Ge Y, Gentry J, Hornik K,

Hothorn T, Huber W, Iacus S, Irizarry R, Leisch F, Li C, Maechler M, Rossini AJ, Sawitzki G, Smith C, Smyth G, Tierney L, Yang JY, Zhang J (2004). Bioconductor: Open software development for computational biology and bioinformatics. *Genome Biol* **5**, R80.

[51] Andrés-Benito P, Moreno J, Aso E, Povedano M, Ferrer I (2017) Amyotrophic lateral sclerosis, gene deregulation in the anterior horn of the spinal cord and frontal cortex area 8: Implications in frontotemporal lobar degeneration. *Aging* **9**, 823-851.

[52] Durrenberger PF, Fernando FS, Magliozzi R, Kashefi SN, Bonnert TP, Ferrer I, Seilhean D, Nait-Oumesmar B, Schmitt A, Gebicke-Haerter PJ, Falkai P, Grünblatt E, Palkovits M, Parchi P, Capellari S, Arzberger T, Kretzschmar H, Roncaroli F, Dexter DT, Reynolds R (2012) Selection of novel reference genes for use in the human central nervous system: A BrainNet Europe Study. *Acta Neuropathol* **124**, 893-903.

[53] Tang WH, Shilov IV, Seymour SL (2008) Nonlinear fitting method for determining local false discovery rates from decoy database searches. *J Proteome Res* **7**, 3661.

[54] Tyanova S, Temu T, Sinitcyn P, Carlson A, Hein MY, Geiger T, Mann M, Cox J (2016) The Perseus computational platform for comprehensive analysis of (prote)omics data. *Nature Methods* **13**, 731-740.

[55] Belzil VV, Bauer PO, Prudencio M, Gendron TF, Stetler CT, Yan IK, Pregent L,Daughrity L, Baker MC, Rademakers R, Boylan K, Patel TC, Dickson DW, Petrucelli L (2013) Reduced C9orf72 gene expression in c9FTD/ALS is caused by histone trimethylation, an epigenetic event detectable in blood. *Acta Neuropathol* **126**, 895-905.

[56] Ciura S, Lattante S, Le Ber I, Latouche M, Tostivint H, Brice A, Kabashi E (2013) Loss of function of C9orf72 causes motor deficits in a zebrafish model of amyotrophic lateral sclerosis. *Ann Neurol* **74**, 180-187.

[57] Xi Z, Zinman L, Moreno D, Schymick J, Liang Y, Sato C, Zheng Y, Ghani M, Dib S, Keith J, Robertson J, Rogaeva E (2013) Hypermethylation of the CpG island near the G4C2 repeat in ALS with a C9orf72 expansion. *Am J Hum Genet* **92**, 981-989.

[58] Waite AJ, Baumer D, East S, Neal J, Morris HR, Ansorge O, Blake DJ (2014) Reduced C9orf72 protein levels in frontal cortex of amyotrophic lateral sclerosis and frontotemporal degeneration brain with the C9ORF72 hexanucleotide repeat expansion. *Neurobiol Aging* **35**, 1779.e5-1779.e13.

[59] Jung J, Behrends C (2017) Multifaceted role of SMCR8 as autophagy regulator. *Small GTPases* **1**, 1-9.

[60] Zhang YJ, Gendron TF, Ebbert MTW, O'Raw AD, Yue M, Jansen-West K, Zhang X, Prudencio M, Chew J, Cook CN, Daughrity LM, Tong J, Song Y, Pickles SR, Castanedes-Casey M, Kurti A, Rademakers R2, Oskarsson B, Dickson DW, Hu W, Gitler AD, Fryer JD, Petrucelli L (2018) Poly(GR) impairs protein translation and stress granule dynamics in C9orf72-associated frontotemporal dementia and amyotrophic lateral sclerosis. *Nat Med* **24**, 1136-1142.

[61] Frick P, Sellier C, Mackenzie IRA, Cheng CY, Tahraoui-Bories J, Martinat C, Pasterkamp RJ, Prudlo J, Edbauer D, Oulad-Abdelghani M, Feederle R, Charlet-Berguerand N, Neumann M (2018) Novel antibodies reveal presynaptic localization of C9orf72 protein and reduced protein levels in C9orf72 mutation carriers. *Acta Neuropathol Commun* **6**, 72.

[62] Kaus A, Sareen D (2015) ALS Patient stem cells for unveiling disease signatures of motoneuron susceptibility: Perspectives on the deadly mitochondria, ER stress and calcium triad. *Front Cell Neurosci* **9**, 448.

[63] Dafinca R, Scaber J, Ababneh N, Lalic T, Weir G, Christian H, Vowles J, Douglas AG, Fletcher-Jones A, Browne C, Nakanishi M, Turner MR, Wade-Martins R, Cowley SA, Talbot K (2016) 9orf72 hexanucleotide expansions are associated with altered endoplasmic reticulum calcium homeostasis and stress granule formation in induced pluripotent stem cell-derived neurons from patients with amyotrophic lateral sclerosis and frontotemporal dementia. *Stem Cells* **34**, 2063-2078.

[64] Palluzzi F, Ferrari R, Graziano F, Novelli V, Rossi G, Galimberti D, Rainero I, Benussi L, Nacmias B, Bruni AC, Cusi D, Salvi E, Borroni B, Grassi M (2017) A novel network analysis approach reveals DNA damage, oxidative stress and calcium/cAMP homeostasis-associated biomarkers in frontotemporal dementia. *PLoS One* **12**, e0185797.

[65] Lau DHW, Hartopp N, Welsh NJ, Mueller S, Glennon EB, Mórotz GM, Annibali A, Gomez-Suaga P, Stoica R, Paillusson S, Miller CCJ (2018) Disruption of ER-mitochondria signalling in fronto-temporal dementia and related amyotrophic lateral sclerosis. *Cell Death Dis* **9**, 327.

[66] Evans CS, Holzbaur ELF (2019) Autophagy and mitophagy in ALS. *Neurobiol Dis* **122**, 35-40.

[67] Ayala V, Granado-Serrano AB, Cacabelos D, Naudí A, Ilieva EV, Boada J, Caraballo-Miralles V, Lladó J, Ferrer I, Pamplona R, Portero-Otin M (2011) Cell stress induces TDP-43 pathological changes associated with ERK1/2 dysfunction: Implications in ALS. *Acta Neuropathol* **122**, 259-270.

[68] Cacabelos D, Ayala V, Granado-Serrano AB, Jové M, Torres P, Boada J, Cabré R, Ramírez-Núñez O, Gonzalo H, Soler-Cantero A, Serrano JC, Bellmunt MJ, Romero MP, Motilva MJ, Nonaka T, Hasegawa M, Ferrer I, Pamplona R, Portero-Otín M (2016) Interplay between TDP-43 and docosahexaenoic acid-related processes in amyotrophic lateral sclerosis. *Neurobiol Dis* **88**, 148-160.

[69] Ilieva EV, Ayala V, Jové M, Dalfó E, Cacabelos D, Povedano M, Bellmunt MJ, Ferrer I, Pamplona R, Portero-Otín M (2007) Oxidative and endoplasmic reticulum stress interplay in sporadic amyotrophic lateral sclerosis. *Brain* **130**, 3111-3123.

[70] Martínez A, Carmona M, Portero-Otin M, Naudí A, Pamplona R, Ferrer I (2008) Type-dependent oxidative damage in frontotemporal lobar degeneration: Cortical astrocytes are targets of oxidative damage. *J Neuropathol Exp Neurol* **67**, 1122-1136.

[71] Ambros V (2004) The functions of animal microRNAs. *Nature* **431**, 350-355.

[72] Bartel DP (2004) MicroRNAs: Genomics, biogenesis, mechanism, and function. *Cell* **116**, 281-297.

[73] Enwerem II, Wu G, Yu YT, Hebert MD (2015) Cajal body proteins differentially affect the processing of box C/D scaRNPs. *PLoS One* **10**, e0122348.

[74] Ransohoff JD, Wei Y, Khavari PA (2018) The functions and unique features of long intergenic non-coding RNA. *Nat Rev Mol Cell Biol 19*, 143-157.

[75] Chow JC, Yen Z, Ziesche SM, Brown CJ (2005) Silencing of the mammalian X chromosome. *Annu Rev Genom Hum Genet* **6**, 69-92.

[76] Ferrer I (2018) Oligodendrogliopathy in neurodegenerative diseases with abnormal protein aggregates: The forgotten partner. *Progr Neurobiol* **169**, 24-54.

[77] Neumann M, Kwong LK, Truax AC, Vanmassenhove B, Kretzschmar HA, Van Deerlin VM, Clark CM, Grossman

M, Miller BL, Trojanowski JQ, Lee VM (2007) TDP-43-positive white matter pathology in frontotemporal lobar degeneration with ubiquitin-positive inclusions. *J Neuropathol Exp Neurol* **66**, 177-183.

[78] Fatima M, Tan R, Halliday GM, Kril JJ (2015) Spread of pathology in amyotrophic lateral sclerosis: Assessment of phosphorylated TDP-43 along axonal pathways. *Acta Neuropathol Commun* **3**, 47.

[79] Bigio EH (2011) C9ORF72, the new gene on the block, causes C9FTD/ALS: New insights provided by neuropathology. *Acta Neuropathol* **122**, 653-655.

[80] Bigio EH (2012) Motor neuron disease: The C9orf72 hexanucleotide repeat expansion in FTD and ALS. *Nat Rev Neurol* **8**, 249-250.

[81] Ferrer I (2017) Diversity of astroglial responses across human neurodegenerative disorders and brain aging. *Brain Pathol* **27**, 645-674.

[82] Kovacs GG, Lee VM, Trojanowski JQ (2017) Protein astrogliopathies in human neurodegenerative diseases and aging. *Brain Pathol* **27**, 675-690.

[83] Prudencio M, Belzil VV, Batra R, Ross CA, Gendron TF, Pregent LJ, Murray ME, Overstreet KK, Piazza-Johnston AE, Desaro P, Bieniek KF, DeTure M, Lee WC, Biendarra SM, Davis MD, Baker MC, Perkerson RB, van Blitterswijk M, Stetler CT, Rademakers R, Link CD, Dickson DW, Boylan KB, Li H, Petrucelli L (2015) Distinct brain transcriptome profiles in C9orf72-associated and sporadic ALS. *Nat Neurosci* **8**, 251175-251182.

[84] Conlon EG, Fagegaltier D, Agius P, Davis-Porada J, Gregory J, Hubbard I, Kang K, Kim D; New York Genome Center ALS Consortium, Phatnani H, Kwan J, Sareen D, Broach JR, Simmons Z, Arcila-Londono X, Lee EB, Van Deerlin VM, Shneider NA, Fraenkel E, Ostrow LW, Baas F, Zaitlen N, Berry JD, Malaspina A, Fratta P, Cox GA, Thompson LM, Finkbeiner S, Dardiotis E, Miller TM, Chandran S, Pal S, Hornstein E, MacGowan DJ, Heiman-Patterson T, Hammell MG, Patsopoulos NA, Dubnau J, Nath A, Phatnani H, Shneider NA, Manley JL (2018) Unexpected similarities between C9ORF72 and sporadic forms of ALS/FTD suggest a common disease mechanism. *Elife* **13**, 7.

[85] Vogel C, Marcotte EM (2012) Insights into the regulation of protein abundance from proteomic and transcriptomic analyses. *Nat Rev Genet* **13**, 227-232.

[86] Marguerat S, Schmidt A, Codlin S, Chen W, Aebersold R, Bähler J (2012) Quantitative analysis of fission yeast transcriptomes and proteomes in proliferating and quiescent cells. *Cell* **151**, 671-683.

[87] Liu Y, Beyer A, Aebersold R (2016) On the dependency of cellular protein levels on mRNA abundance. *Cell* **165**, 535-550.